Ntritsos, N. *et al. Géotechnique* [http://dx.doi.org/10.1680/geot.14.P.205]

Static and cyclic undrained response of square embedded foundations

N. NTRITSOS*, I. ANASTASOPOULOS† and G. GAZETAS‡

Results of a three-dimensional finite-element study for the effect of embedment on the undrained bearing capacity, the elastic stiffness, and the cyclic behaviour of square-in-plan foundations are presented. Uniaxial horizontal (Q) and pure-moment (M) limit loads, as well as the respective elastic stiffnesses (K_{HH} and K_{MM}) are obtained, and simplified models are developed to interpret the observed trends. The substantially different role of embedment in increasing elastic stiffness and in increasing ultimate loads is interpreted in simple soil mechanics terms. Extensive comparisons are made with the two-dimensional results for a strip foundation. Combined (QM) loading capacities are obtained and presented as 'interaction' diagrams; the significance of the vertical load (N) is also addressed. The importance of the type of contact between the foundation interfaces (vertical or horizontal) with the surrounding or underlying soil is explored. A substantial reduction in all capacities is shown when the interfaces are tensionless and of limited shear (sliding) resistance (TSI), compared with the capacities for the ideal case of fully bonded contact (FBC). The cyclic moment–rotation (M–θ) response of embedded foundations carrying a simple slender structure is investigated parametrically. It is found that the monotonic loading curves provide approximately the envelope for the cyclic M–θ loops. But the shape of these loops and the ensuing settlement of the foundation are both functions of the factor of safety (FS_V) against vertical bearing capacity. In case of surface and shallowly embedded foundations with high values of FS_V (i.e. with light loading or on very stiff soil) the loops pass nearly through the centre ($M=\theta=0$) of the coordinate axes and the residual settlement is negligible; both are a consequence of the predominantly geometric non-linearity in the form of separation of the walls and uplifting of the base from the soil. On the contrary, with low FS_V values (heavy loading or soft soil) *and* deeper relative embedment, broad hysteresis loops and accumulating settlement are the rule – a product of material inelasticity of the soil, under limited soil–foundation detachment.

KEYWORDS: bearing capacity; failure; finite-element modelling; footings; foundations; soil/structure interaction; stiffness

INTRODUCTION

Static foundation design calls for avoiding failure of the soil–foundation system, and ensuring that the system displacements will be compatible with the desired structural performance. Prediction of the ultimate 'failure' loads of a foundation has traditionally been addressed in practice with the conventional bearing capacity theory (Terzaghi, 1943; Meyerhof, 1953; Brinch Hansen, 1970). The basis of this theory is the algebraic expression of the ultimate vertical load N_u as a function of the soil strength parameters, the soil mass density and the foundation geometry. When vertical, horizontal and moment loading act simultaneously on the foundation, to obtain the ultimate condition a series of 'reduction' factors for inclination and eccentricity are applied to N_u. The effect of embedment is incorporated in the bearing capacity expression with the use of semi-empirical depth factors increasing the capacity over that of the surface footing with the same base geometry. Although this traditional approach has gained widespread acceptance in foundation engineering practice, its quasi-empirical nature renders it just an approximation. Moreover, it cannot be directly used in numerical one-step soil–structure interaction analyses, as explained by Houlsby (2003). To overcome drawbacks, many researchers (Butterfield & Ticoff, 1979; Georgiadis & Butterfield, 1988; Nova & Montrassio, 1991; Butterfield & Gottardi, 1994; Martin, 1994; Salencon & Pecker, 1995; Bransby & Randolph, 1999; Gottardi *et al.*, 1999; Houlsby & Puzrin, 1999; Taiebat & Carter, 2000; Houlsby, 2003; Randolph & Puzrin, 2003; Gourvenec, 2007, 2008; Yun & Bransby, 2007; Chatzigogos *et al.*, 2009; Randolph & Gourvenec, 2011) have developed the concept of a 'failure envelope' which in a Cartesian coordinate system with axes the vertical force, N, the horizontal force, Q, and the overturning moment, M, is the surface that indicates bearing capacity failure for all possible NQM load combinations. When the point representing a particular load combination plots inside this 'failure envelope', the foundation does not fail; when just touching the envelope, it mobilises a 'failure' mechanism and deforms inelastically.

On the other hand, seismic design of soil–foundation–structure systems requires knowledge of the elastic or quasi-elastic stiffnesses of the foundation, since these more-or-less control the natural frequencies of the system, and hence the loads that are transmitted from the structure to the foundation. A significant effort has been spent on obtaining static and dynamic stiffnesses of foundations; a wealth of results has been published in the last 40 or more years, for both uniaxial and combined loading on various idealised soil profiles: compilations of such solutions have appeared in papers by Roesset (1980), Gazetas (1983), Dobry & Gazetas (1986), Pais & Kausel (1988) and Wolf (1988). The effect of foundation embedment on stiffnesses has been studied numerically, but expressed in a similar way as for the bearing capacity: using closed-form depth-of-embedment

Manuscript received 10 October 2014; revised manuscript accepted 28 May 2015.
Discussion on this paper is welcomed by the editor.
* UME School, IUSS Pavia, Italy; formerly National Technical University of Athens, Athens, Greece.
† University of Dundee, Dundee, UK; formerly National Technical University of Athens, Athens, Greece.
‡ National Technical University of Athens, Athens, Greece.

'correction' factors to enhance the stiffnesses over those of the surface footing with the same base geometry (Kausel & Roesset, 1975; Tassoulas & Kausel, 1983; Wolf, 1985, 1988; Gazetas, 1991). The historical developments in this soil–foundation interaction field (albeit from a dynamic point of view) have been presented recently by Kausel (2010), while Dobry (2014) has compiled a wealth of solutions obtained with simple, physically inspired methods.

In the last 10 or 15 years, studies of dynamic soil–foundation–structure interaction have explored the idea that under seismic (base) excitation mobilising the ultimate capacity of foundations may be beneficial for the whole system. The concept of 'rocking isolation' has thereby emerged as an alternative to the conservative – yet not safer – design of foundations against strong seismic shaking (Pecker, 1998; Martin & Lam, 2000; Faccioli *et al.*, 2001; Paolucci *et al.*, 2008; Gajan & Kutter, 2008; Anastasopoulos *et al.*, 2010a, 2012; Gazetas, 2015). As a result of these studies, the response of foundations under cyclic loading mobilising the ultimate capacities has become a key part of the seismic foundation design – bridging the gap between static and dynamic analysis.

Studies of the ultimate response of embedded foundations refer mostly to strip and circular foundations, the external surfaces of which are perfectly 'glued' to the soil (Bransby & Randolph, 1999; Poulos *et al.*, 2001; Yun & Bransby, 2007; Gourvenec, 2008). These studies have focused mainly on the undrained bearing capacity under combined loading, modelling the soil as an elastoplastic continuum. Recent studies treating the soil as an inelastic and tensionless Winkler medium include those by Allotey & Naggar (2003) and Gerolymos & Gazetas (2006a, 2006b, 2006c).

The aim of the current study is to extend previous work in an effort to quantify the inelastic response of embedded foundations. A series of three-dimensional (3D) finite-element (FE) analyses are reported treating the soil as an elastoplastic continuum in order to investigate

(*a*) the effect of embedment on the undrained capacity of square-in-plan foundations under combined loading for a fully bonded contact (FBC) of the foundation with the soil; simple analytical solutions offer enhanced understanding of the mechanics of the problem
(*b*) the effect of having a tensionless interface of limited shear capacity (TSI) on the failure envelopes of an embedded foundation
(*c*) the effect of embedment on the elastic stiffnesses in rotation and horizontal translation of the foundation in FBC with the soil; and the relationship of the effects of embedment on (i) bearing capacity and (ii) stiffness
(*d*) the rotational ('rocking') response of simple but slender structures on embedded foundations under monotonic and cyclic displacement-controlled loading, driving them to large deformations after their moment capacity is reached.

Square foundations of various embedment ratios ($0 \leq D/B \leq 1$) are considered under undrained loading conditions. As depicted in Fig. 1 the problem is analysed in two different phases. First (Fig. 1(a)), the bearing capacity of the soil–foundation system is examined under combined monotonic MQ loading applied directly at the foundation base level, not accounting for second-order phenomena. Failure envelopes are predicted in typical sections of the 3D load space.

In the second part (Fig. 1(b)), the entire soil–foundation–structure system is modelled, where the superstructure is represented by a rigid beam element with a lumped mass at its top. The system is subjected to monotonic and cyclic horizontal loading applied at the level of the lumped mass. The load combinations are compatible with the slenderness of the superstructure (i.e. the beam length) and P–Δ effects are taken into account. Emphasis is placed on the failure mechanisms, the comparison between the effects of embedment on stiffness and capacity, the cyclic behaviour and the residual deformations of the foundation.

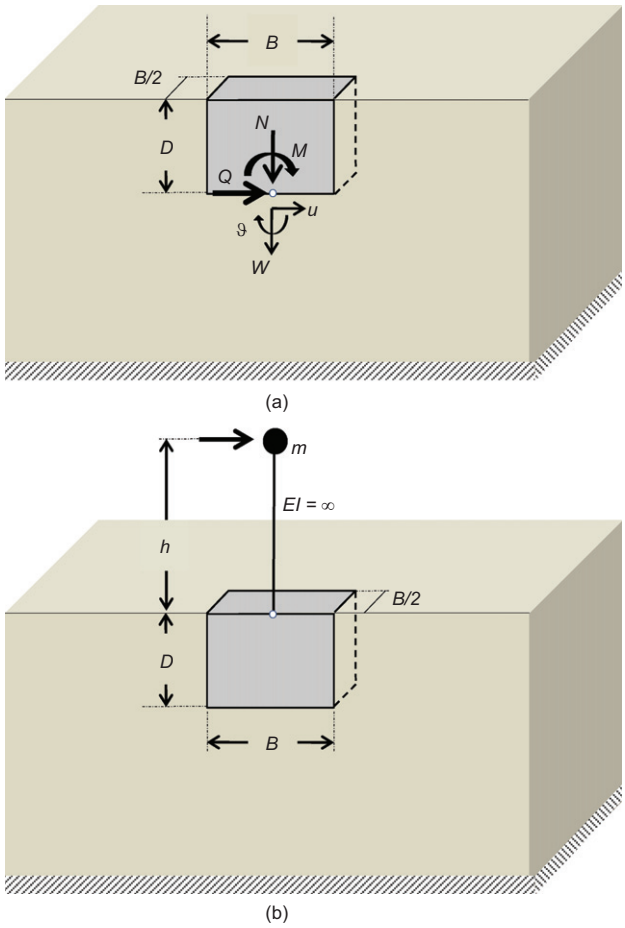

Fig. 1. Problem definition and symbols: (a) soil–foundation system (load and displacement reference point at the base of the foundation); (b) soil–foundation–structure system (load and displacement reference point at base of structure (top of foundation))

Finite-element modelling

A series of 3D FE analyses are performed using Abaqus (2008). A typical 3D FE mesh, taking advantage of problem symmetry, is shown in Fig. 2. Soil and foundation are modelled with eight-noded hexahedral brick-type elements,

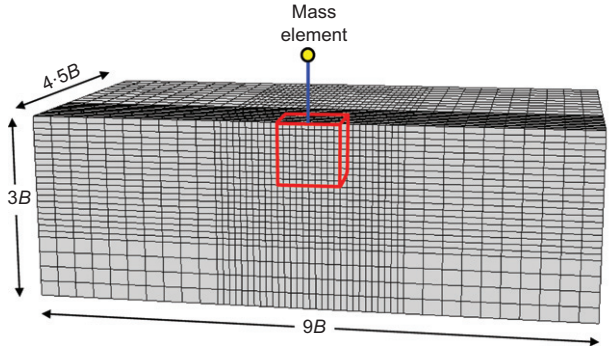

Fig. 2. Outline and dimensions of three-dimensional FE model

non-linear for the former and elastic for the latter. Fully integrated first-order isoparametric elements are employed for this purpose, in which the volume changes at Gauss points are replaced by the average volume change of the element. Such selective reduced integration (because the order of integration is reduced in selected terms) helps prevent mesh locking, providing accurate solutions even in (nearly) incompressible materials. Its efficiency has been verified in previous publications (e.g. Gazetas *et al.*, 2013), and through initial sensitivity and benchmark analyses for the specific problem analysed herein.

The soil is a homogeneous clay stratum modelled as an elastoplastic material (with parametrically variable undrained shear strength $S_u = 75$–150 kPa, $E/S_u = 1800$, $\gamma = 20\,\mathrm{kN/m^3}$) while the foundation is modelled invariably as a rigid body. The base of the model is fixed in all three coordinate directions. Special interface elements are used for the soil–foundation interface, modelling two different conditions as ('artistically') sketched in Fig. 3.

(*a*) Fully bonded contact (FBC): this is where the foundation is assumed to remain in perfect contact with the surrounding soil (Fig. 3(a)). Such contact has infinite tensional and shear capacities, preventing separation and slippage of the foundation from the soil.
(*b*) Tensionless sliding interface (TSI): in this case, separation (gapping) of the foundation from the soil, as well as slippage at the soil–foundation interface, are permitted (Fig. 3(b)). The latter obeys in total stress analysis Coulomb's friction law with $\varphi_a = 0$ and $c_a = \alpha S_u$, while detachment and uplifting arise from the tensionless interface behaviour. In the analyses presented herein, the adhesion coefficient, α, was set equal to 0·80.

Soil modelling

The non-linear soil behaviour is modelled through a simple kinematic hardening model with Von Mises failure criterion and associated flow rule. The evolution law of the model consists of two components: a non-linear kinematic hardening component which describes the translation of the yield surface in the stress space (defined through a 'back-stress' parameter β), and an isotropic hardening component which defines the size of the yield surface σ_0 as a function of plastic deformation. The pressure-independent yield surface of the model according to the Von Mises failure criterion is defined through the following function F

$$F = f(\sigma - \beta) - \sigma_0 \tag{1}$$

The model hinges on three parameters: the elastic Young's modulus E, the ultimate strength σ_u and the yield stress σ_0. The evolution of the kinematic component of the yield stress is defined as

$$\dot{\alpha} = C\frac{1}{\sigma_0}(\sigma - \alpha)\dot{\varepsilon}^{pl} - \gamma\alpha\dot{\varepsilon}^{pl} \tag{2}$$

where C is the initial kinematic hardening modulus ($C = \sigma_y/\varepsilon_y = E = 2(1+\nu)G_o$) and γ is a parameter determining the rate of decrease of the kinematic hardening with increasing plastic deformation. In the case of clay, the maximum yield stress can be defined as

$$\sigma_y = \sqrt{3}S_u \tag{3}$$

And since $\sigma_y = C/\gamma + \sigma_0$, parameter γ can be expressed as

$$\gamma = \frac{C}{\sqrt{3}S_u - \sigma_0} \tag{4}$$

Parameter σ_0 controls the initiation of non-linear behaviour and is defined as a fraction λ of the yield stress σ_y

$$\sigma_0 = \lambda\sigma_y \tag{5}$$

Finally, C corresponds to the Young's modulus for very small strains.

Details on the calibration of the model parameters from published experimental G–γ and ξ–γ curves (Vucetic & Dobry, 1991), and the reasonably satisfactory comparisons of its predictions against centrifuge model tests and analytical solutions, can be found in papers by Anastasopoulos *et al.* (2011, 2012) and Adamidis *et al.* (2014). In all the analyses, the calibration of parameters was based on the Vucetic & Dobry (1991) G–γ curves for plasticity index of the soil, PI = 30.

Loading conditions

In the first phase (see Fig. 1(a)), displacement-controlled monotonic loading was applied directly at the centre of the foundation base. A fraction of the ultimate vertical bearing capacity N_u was imposed as a direct vertical force N, followed by a displacement probe of constant ratio u/θ until the foundation load does not vary with increased displacement. In the words of Yun & Bransby (2007): 'once the failure envelope is reached, each loading path travels around the failure envelope until it reaches a termination point where the direction of the tangent to the failure envelope matches the prescribed displacement ratio'. As associative flow rule was assumed in the constitutive model, the failure envelope serves also as the plastic potential surface, with the direction of the incremental plastic displacement vector at failure being perpendicular to that surface.

It is noted here that the selection of the load reference point affects significantly the shape of the failure envelope produced. In this paper the failure envelopes refer to the centre of the foundation base, in order to be compatible with numerous already published results.

Model validation

The constitutive model has been validated against physical model tests (centrifuge, 1***g***, and large scale) for: (*a*) surface and embedded foundations subjected to cyclic loading and seismic shaking (Anastasopoulos *et al.*, 2011, 2012); (*b*) piles subjected to cyclic loading (Giannakos *et al.*, 2012); (*c*) bar-mat retaining walls subjected to seismic shaking (Anastasopoulos *et al.*, 2010b); and (*d*) circular tunnels subjected to seismic shaking (Bilotta *et al.*, 2014; Tsinidis *et al.*, 2014). The latter two offer an independent validation, as part of a carefully planned round robin numerical test using centrifuge model tests conducted at the University of Cambridge (Lanzano *et al.*, 2012). Despite its simplicity, the model was shown to perform very well, in many cases outperforming more sophisticated models (Bilotta *et al.*, 2014).

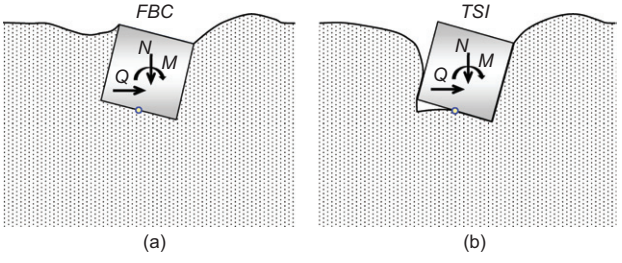

Fig. 3. Sketched representation for the meaning of soil–foundation interface conditions: (a) FBC; (b) tensionless and potentially sliding interface – TSI

The model is further validated herein against published failure envelopes for embedded foundations subjected to combined NQM loading. As mentioned earlier, most of the available solutions are limited to plane-strain conditions. For a meaningful comparison, the 3D FE model of Fig. 2 is transformed into an equivalent two-dimensional (2D) model by considering only an appropriate 'slice'. A FBC is considered: sliding or detachment is disallowed. Several analyses were conducted using different u/θ ratios to produce the failure envelope for a certain plane in NQM loading space. Fig. 4(a) shows the load paths for different displacement probes in comparison with the respective failure envelope of Gourvenec (2008) for an embedment ratio $D/B=1$. To the present authors' satisfaction, the terminal points of the load paths fall on top of, or sufficiently close to, Gourvenec's envelope. An additional validation for $D/B=0{\cdot}5$ against the failure envelope of Vulpe *et al*. (2014) for circular foundations and Gourvenec (2008) for strip foundations is shown in Fig. 4(b).

NUMERICAL AND (SOME) ANALYTICAL RESULTS

The undrained bearing capacity of rigid embedded strip foundations under combined NQM loading has been extensively investigated by, among others, Yun & Bransby (2007) and Gourvenec (2008), who considered plane-strain (2D) conditions and a fully bonded soil–foundation contact. The current study extends these results: (*a*) to the 3D problem of a square embedded foundation; and (*b*) to the case of a tensionless interface which accommodates both separation and sliding (the latter when a certain fraction, $\alpha=0{\cdot}80$, of the soil undrained shear strength is reached: $f_S=0{\cdot}80\ S_u$); (*c*) to the comparative study of the influence of embedment on stiffness against that on ultimate capacity; and (*d*) to the response under quasi-static cyclic loading coming from lateral loading on top of a slender structure.

FULLY BONDED CONTACT

Lateral bearing capacity and elastic stiffness

Numerical results from the 3D FE analysis (FEA) of square-in-plan embedded foundations are presented and compared with those of the corresponding plane-strain analyses. Thanks to the additional two side surfaces, parallel to the direction of loading, the square foundation enjoys increased soil resistance beyond the one experienced by an equivalent embedded strip (2D) foundation – for all modes of loading: vertical, horizontal and moment. Furthermore, the

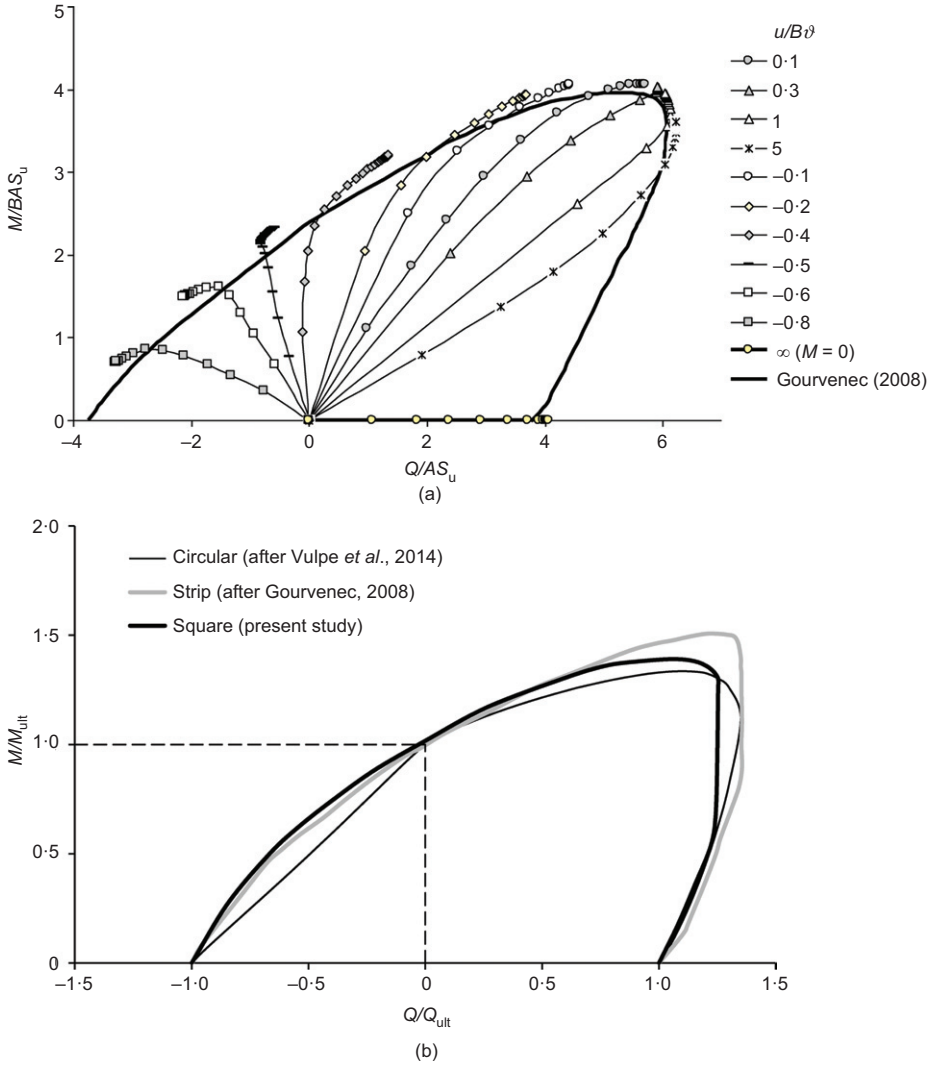

Fig. 4. (a) Model validation for the two-dimensional plane-strain problem with $D/B=1$ and $N/N_{ult}=0{\cdot}5$: comparison of the MQ failure envelope of Gourvenec (2008) (continuous line) with the terminal points of probe lines (of constant $u/B\theta$) of the present analysis. (b) Model validation for $D/B=0{\cdot}5$ and $N/N_{ult}=0{\cdot}5$: comparison of the MQ failure envelope of the present study to that of Vulpe *et al.* (2014) for circular foundations and Gourvenec (2008) for strip foundations

unavoidable three-dimensionality of the failure mechanism elicits increased soil resistance, as explained below.

Horizontal translation (without rotation). A simple failure mechanism aimed merely at illustrating the origin of the effect of embedment is depicted in Fig. 5. The lateral bearing capacity Q_{max} of a square embedded footing is examined under pure horizontal translation (rotation $\theta=0$). In two dimensions the foundation ultimate horizontal capacity ${}^{2d}Q_{max}$ could be obtained roughly as the superposition of the ultimate base shear (${}^{2d}Q_{base}$), which is essentially equal to the ultimate shear force ${}^{2d}Q_{uo}$ of a surface footing (${}^{2d}Q_{uo} \approx {}^{2d}Q_{base} \approx S_u A_{base}$) and the passive-minus-active force (${}^{2d}P_{passive} - {}^{2d}P_{active}$) obtained from Coulomb-type plane-strain analysis (here assuming a circular sliding surfaces motivated by the FE observations of, say, Fig. 9). For such type of analysis (but using a rigorous method) Gourvenec (2008) has fitted the following expression to the numerical results for the maximum horizontal load as a multiple of the corresponding load of the surface footing

$$ {}^{2d}Q_{max} \approx {}^{2d}Q_{uo}[1 + 5{\cdot}56(D/B)] \tag{6}$$

Interestingly, for the elastic horizontal stiffness of a strip foundation, the effect of embedment is much less significant (Gazetas, 1983, as modified recently by Lekkakis, 2012)

$$ {}^{2d}K_H \approx {}^{2d}K_{HO}[1 + 1{\cdot}2(D/B)] \tag{7}$$

For example, for $D/B=1$, the increase in stiffness due to embedment is only about 1/3 of the corresponding increase in bearing capacity. Here are two possible culprits of such a greater effect of embedment on ultimate load as opposed to its effect on stiffness.

(*a*) The most significant: the sidewall (vertical) surfaces at small elastic deformations invoke a disproportionately small soil reaction; because each sidewall can be viewed as nothing more than a vertical strip at the edge of a homogeneous quarter-space (i.e. the space between the horizontal surface from the footing edge to infinity along the x-axis, and the vertical axis passing along the sidewall, as sketched in the insert of Fig. 5); that strip is loaded horizontally (i.e. perpendicularly to its surface). Recall that on a homogeneous half-space the normal

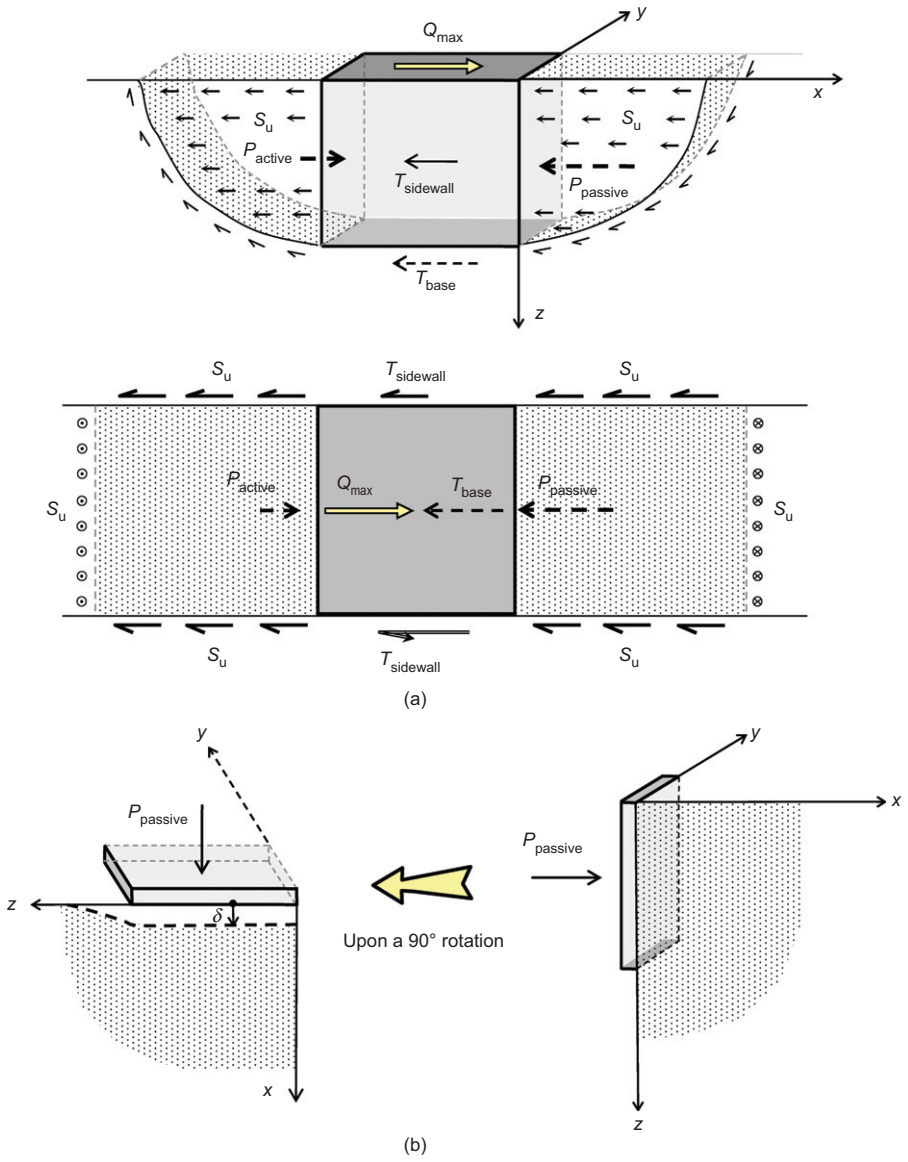

Fig. 5. (a) Estimation of maximum horizontal capacity of three-dimensional embedded foundations with finite plan dimensions: isolation of a slice of soil which slides against the surrounding soil. (b) Sketch illustrating the role of the sidewall that is normal to the direction of loading

stiffness, K_v, of a strip is vanishingly small. It will be even smaller on a quarter-space. This is because on a homogeneous half-space an infinitely long and uniformly loaded strip leads exactly to infinite displacement – vertical or horizontal, depending on the loading direction (normal or shear). Hence K_v (or K_H)$\rightarrow$0. This is an unequivocal result (a fact) of the theory of elasticity. Naturally, in real life neither a homogeneous half-space (i.e. a homogeneous medium of infinite depth) nor a strip loading (i.e. of infinite extent) can exist. The soil will become inhomogeneous or meet a stiff soil layer or rock at some depth, H. In such a case K_v decreases as H/B increases. But this has nothing to do with the idealisation of the embedded foundation – the side soil extends to infinity in the horizontal direction. By contrast, the (Coulomb-type) sliding wedge is of limited extent, and the resulting passive resistance is relatively huge (requiring of course a very large deformation). The 'true' failure mechanism from the FEA, to be discussed later in this paper, elucidates this point. Hence the much greater contribution of the side walls to the overall foundation capacity rather than stiffness.

(*b*) The small-deformation elastic regions below the base and in front of the sidewalls affect each other (a base-to-side interaction), thus reducing the overall stiffness to a smaller value than what the summation of their effects would provide; at failure, however, the mechanism comprises three more-or-less independent sliding surfaces, and therefore the ultimate load is essentially the sum of the respective three resistances.

Now, under 3D conditions, two additional foundation sidewalls are available, parallel to the loading plane resisting in pure shear the horizontal translation. The maximum additional force is given by

$$T_{\text{sidewall}} \approx S_u A_{\text{sidewall}} = 2 \times B\,D S_u \tag{8}$$

Furthermore, the simple mechanism of Fig. 5 consists of two quarter-cylinder Coulomb-type sliding wedges, as would have also been appropriate for the 2D problem; but now, additionally, the four sides of the two cylinders experience shear stresses S_u from the outside un-deforming soil. Hence the passive-minus-active force increases by

$$F_{\text{sidesoil}} \approx S_u \pi D^2/4 \times 4 = S_u \pi D^2 \tag{9}$$

Therefore, assuming for simplicity that the three partial mechanisms act independently, an upper-bound estimate for the maximum horizontal force of the square-in-plan embedded foundation would be

$$\begin{aligned} Q_{\max}/Q_{\text{uo}} &\approx Q_{\max}/B^2 S_u \\ &\approx [1 + 5{\cdot}56(D/B)] + [2(D/B)] + [\pi(D/B)^2] \end{aligned} \tag{10}$$

in which $Q_{\text{uo}} \approx B^2 S_u$ is the ultimate horizontal capacity of a surface square foundation. Fig. 6 compares the $Q_{\max}/B^2 S_u$ plotted against D/B relationship from the FEA with the above approximate expression. Given the simplicity of the failure mechanism (hardly optimised) for the passive and active resistance, equation (10) is surprisingly (and perhaps fortuitously) accurate.

Admittedly, however, whereas equation (10) is independent of the vertical load N acting on the foundation, the FEA gives results that are slightly affected by the vertical load N. This explains the approximate equality sign between

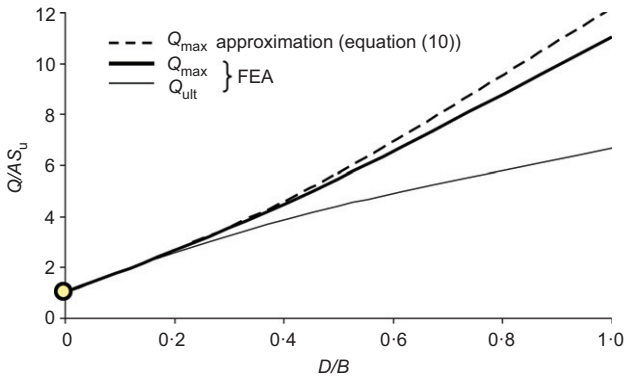

Fig. 6. The two horizontal capacities $Q_{\max}$ (zero rotation) and Q_{ult} (zero moment) from the FE analysis and the simplified model, as functions of the embedment ratio D/B. FBC, $N=0$

Q_{uo} and $B^2 S_u$ in the above expressions. In fact, although not thoroughly reported in this paper, relevant numerical simulations show that the effect of vertical load becomes significant only progressively (with increasing N) when approximately

$$N > 3B^2 S_u \approx N_{\text{uo}}/2 \tag{11}$$

in which N_{uo} is the ultimate vertical capacity of the surface foundation, as it will be shown subsequently. As an example, for $D/B=1$, notice in Fig. 6 (as well as in equation (10)) that

$$Q_{\max}/B^2 S_u \approx Q_{\max}/Q_{\text{uo}} \approx 11{\cdot}5 \tag{12}$$

which is a very substantial effect, indeed.

Again, compare the above with the elastic horizontal stiffness of a square-in-plan foundation with the same embedment $D/B=1$ (Gazetas, 1991; Lekkakis, 2012)

$$\begin{aligned} K_H/K_{HO} &\approx [1 + 0{\cdot}21(D/B)^{0{\cdot}5}][1 + 1{\cdot}57(D/B)^{0{\cdot}8}] \\ &\approx 3{\cdot}1 \end{aligned} \tag{13}$$

where

$$K_{HO} \approx 9GB/(2-\nu) \tag{14}$$

is the elastic horizontal stiffness of the surface square foundation. Notice that, once more, the effect of embedment on the horizontal stiffness is an even smaller fraction (about 1/4) of the effect on ultimate load. The explanation is as above for the 2D problem, but with four rather than two sidewall surfaces participating now. Fig. 7(a) illustrates the (purely horizontal) failure mechanism for two embedment ratios (0·2 and 1), in the form of the vectors of displacement, with superimposed as dark shadows the regions of large plastic strains. It is interesting to observe that the plastic strains tend to localise in well-defined shear bands. In such cases, the problem can be mesh dependent and a sensitivity analysis is required. Such a sensitivity study was performed as part of the present study, leading to the selection of the adopted FE mesh.

Rotation about the centre of the base. The overturning moment, $M_{\max}$, producing a rotational failure without horizontal displacement, is similarly affected by the presence of the sidewalls that are perfectly bonded to the surrounding soil. Fig. 8 plots the variation of $M_{\max}/BAS_u$ against D/B from the FEA.

To compare the 3D results of this figure with the 2D effects of embedment, recall again the plane-strain analysis of Gourvenec (2008), who has fitted the following expression to her numerical results for the maximum

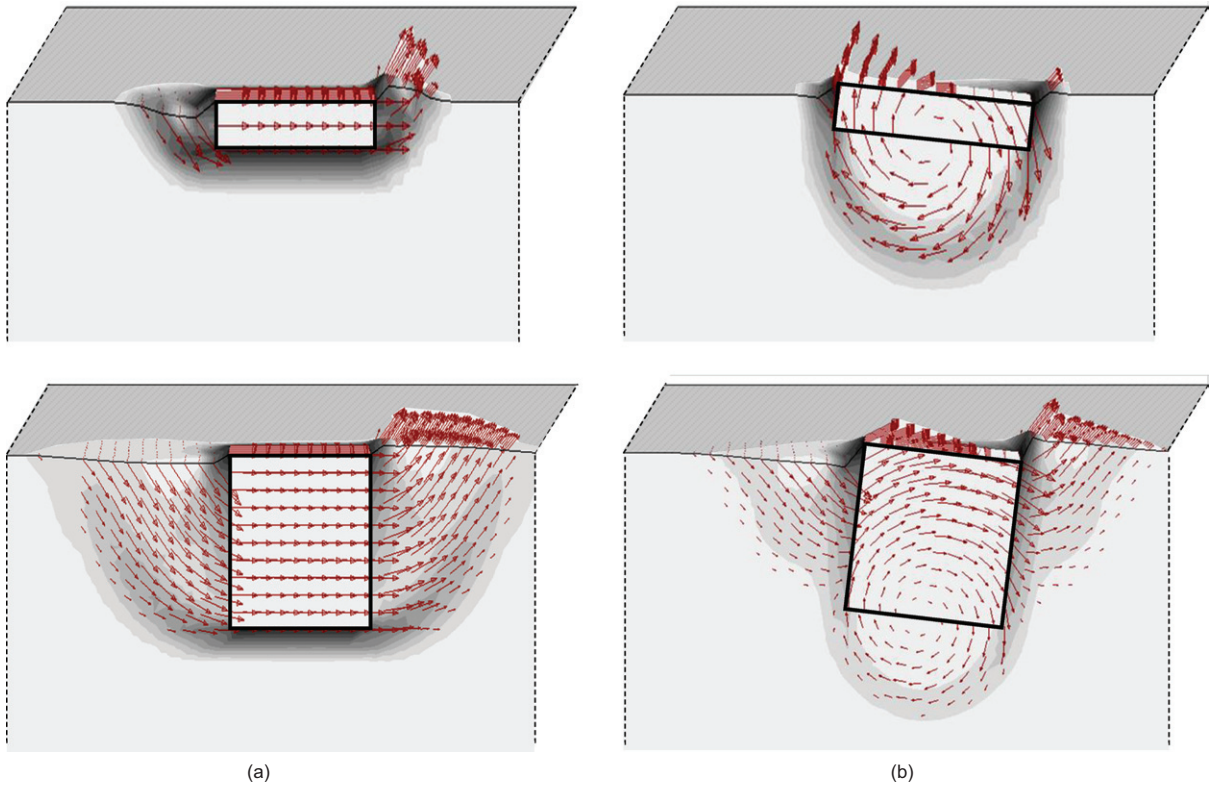

Fig. 7. Displacement vectors at two failure loads: (a) at Q_{max} (with zero rotation); (b) at M_{max} (with zero horizontal displacement). Top row: $D/B = 0{\cdot}2$; bottom row $D/B = 1$. Grey shades indicate the location of high concentration of shear strains, revealing the failure mechanisms. FBC

moment

$$^{2d}M_{max} \approx ^{2d}M_{uo}[1 + 1{\cdot}59(D/B) + 3{\cdot}22(D/B)^2] \quad (15)$$

where $^{2d}M_{uo}$ is the ultimate moment of the fully bonded surface strip foundation.

As an example, for $D/B = 1$, equation (15) yields an ultimate moment ratio $^{2d}M_{max}/^{2d}M_{uo} \approx 5{\cdot}8$. This can be compared with the effect of embedment on the elastic rotational stiffness of a strip foundation

$$^{2d}K_R/^{2d}K_{RO} \approx 1 + 2(D/B) = 3 \quad (16)$$

where the rotational stiffness of the surface strip (per unit running length) is

$$^{2d}K_{RO} = \pi GB^2/[8(1 - \nu)] \quad (17)$$

The effect of embedment on stiffness is now more substantial, but still about 1/2 of the effect on ultimate rotational capacity. The cause of this increased relative importance of embedment on stiffness will be discussed and explained below.

The 3D square-in-plan embedded foundation studied here would potentially benefit from the following additional contributions to resistance over and above the embedded strip footing.

(*a*) The base now is square rather than strip; the failure mechanism is different and the ultimate pure moment of the fully bonded footing is approximately

$$M_{uo} \approx S_u BA \quad (18)$$

(*b*) The two sidewalls that are parallel to the direction of loading undergo a torsional-type movement about the horizontal axis passing from the centre of the base, thus contributing by an amount

$$M_{T,sidewall} \approx S_u BD \times D/2 \times 2 = S_u BD^2 \quad (19)$$

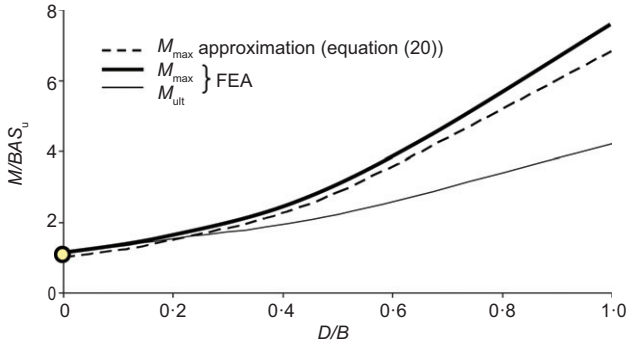

Fig. 8. The two moment capacities M_{max} (zero horizontal displacement) and M_{ult} (zero horizontal force) from the FE analysis and the simplified model, as functions of the embedment ratio D/B. FBC, $N = 0$

(*c*) The two sidewalls that are perpendicular to the loading direction undergo a movement which can decomposed into a vertical and a horizontal translation of their centre, equal to $\theta B/2$ and $\theta D/2$, respectively, and rotation θ around their centroidal horizontal axis (rocking). Of these, the vertical movement invokes shear resistance and its ultimate value $A_{sidewall}S_u$ is the same, equal to $2 \times BDS_u$, for the strip and the square. Hence no correction above what applies to the strip is needed. For the rotation and the horizontal compression, the aforementioned correction shape factor of 1·2 would arguably be an upper bound above what applies to the strip. Hence, assuming for now independence of each contributing movement, gives as an average the factor: $(1 + 1{\cdot}2 + 1{\cdot}2)/3 \approx 1{\cdot}13$. In fact, since some interplay among these three components of ultimate resistance is unavoidable, this small correction factor will be ignored altogether, accepting that the second factor on the right-hand side of

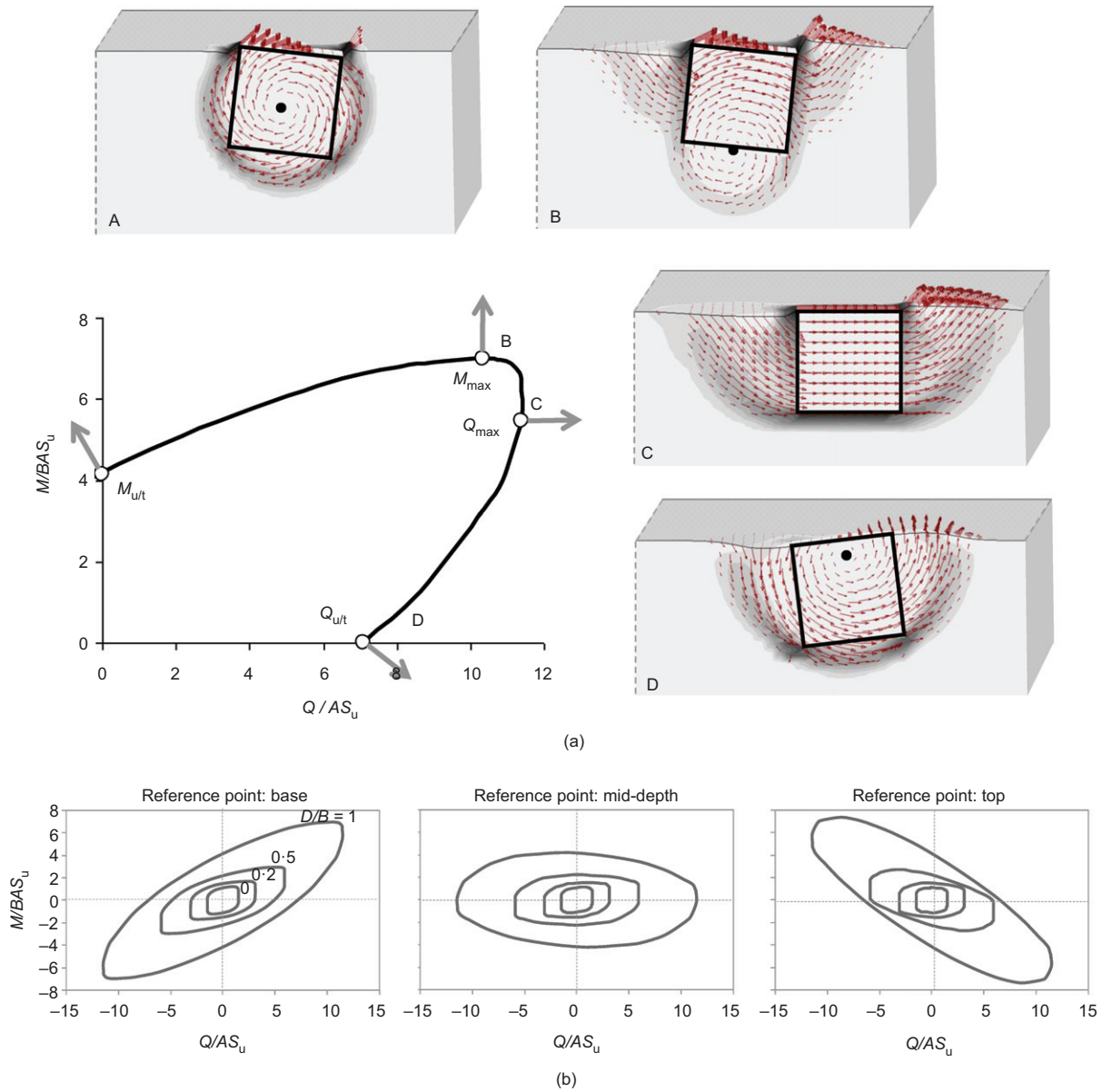

Fig. 9. (a) MQ interaction envelope with the direction of plastic deformations at four key points, along with displacement vectors and concentration of shear strains revealing the failure mechanisms at the above four points. FBC, $D/B=1$. The solid dots in the pictures represent the instantaneous rotation pole of the foundation. (The pole is at infinity for the horizontal translation case, C.) (b) Change of the form of the interaction MQ diagrams by changing the reference point (left: foundation base (see Fig. 1) as with the previous figures; middle: centre of gravity (mid-depth) of the foundation; right: foundation top surface)

Gourvenec's equation (15) adequately describes the contribution of the two perpendicular sidewalls. Hence, as a crude approximation, the maximum moment is

$$M_{\max} \approx M_{\text{uo}}[1 + 1{\cdot}59(D/B) + 4{\cdot}22(D/B)^2] \qquad (20)$$

which for the example of $D/B=1$ gives for the normalised moment: $M_{\max}/M_{\text{uo}} \approx 6{\cdot}8$. In Fig. 8 the FEA gives a larger value, 7·5. Given the crudeness of the above simple upper-bound analysis, its performance is quite acceptable.

Again it is worth comparing the above with the effect of embedment on the elastic rotational stiffness of the foundation for $D/B=1$. From the aforementioned publications

$$K_{\text{R}}/K_{\text{RO}} \approx \{1 + 1{\cdot}3(D/B)[1 + (D/B)]\} \approx 3{\cdot}6 \qquad (21)$$

It is quite interesting to notice that the effect of embedment on stiffness for this mode of loading is about 0·60 times the corresponding effect on the ('true') bearing capacity.

Table 1 compiles the above comparisons between the aforementioned effects of embedment on capacity and stiffness for horizontal and rotational loading. It is clear that in both 2D (strip) and 3D (square) situations

(*a*) the rotational stiffness increases approximately by 1/2 to 2/3 as much as the increase in maximum (overturning) moment
(*b*) the horizontal stiffness increases approximately by only 1/4 to 1/3 as much as the increase in maximum (horizontal) force.

A simple explanation for the relatively increased effect on the rotational stiffness could be unravelled from the previous discussion: any rectangular footing of width B on a halfspace subjected to moment loading (in rocking or torsion) affects only a limited volume of soil; in the traditional geotechnical jargon, it produces elastic 'stress bulbs' of very limited

Table 1. Comparison of the effects of embedment on ultimate loads and elastic stiffnesses for square (Q, K) and strip (^{2d}Q, ^{2d}K) foundations: results of FEA. $D/B=1$

$^{2d}Q_{max}/^{2d}Q_{uo}$	$^{2d}K_H/^{2d}K_{HO}$	Q_{max}/Q_{uo}	K_H/K_{HO}	$^{2d}M_{max}/^{2d}M_{uo}$	$^{2d}K_R/^{2d}K_{RO}$	M_{max}/M_{uo}	K_R/K_{RO}
6·6	2·3	11·5	3·1	5·8	3·0	7·5	3·6

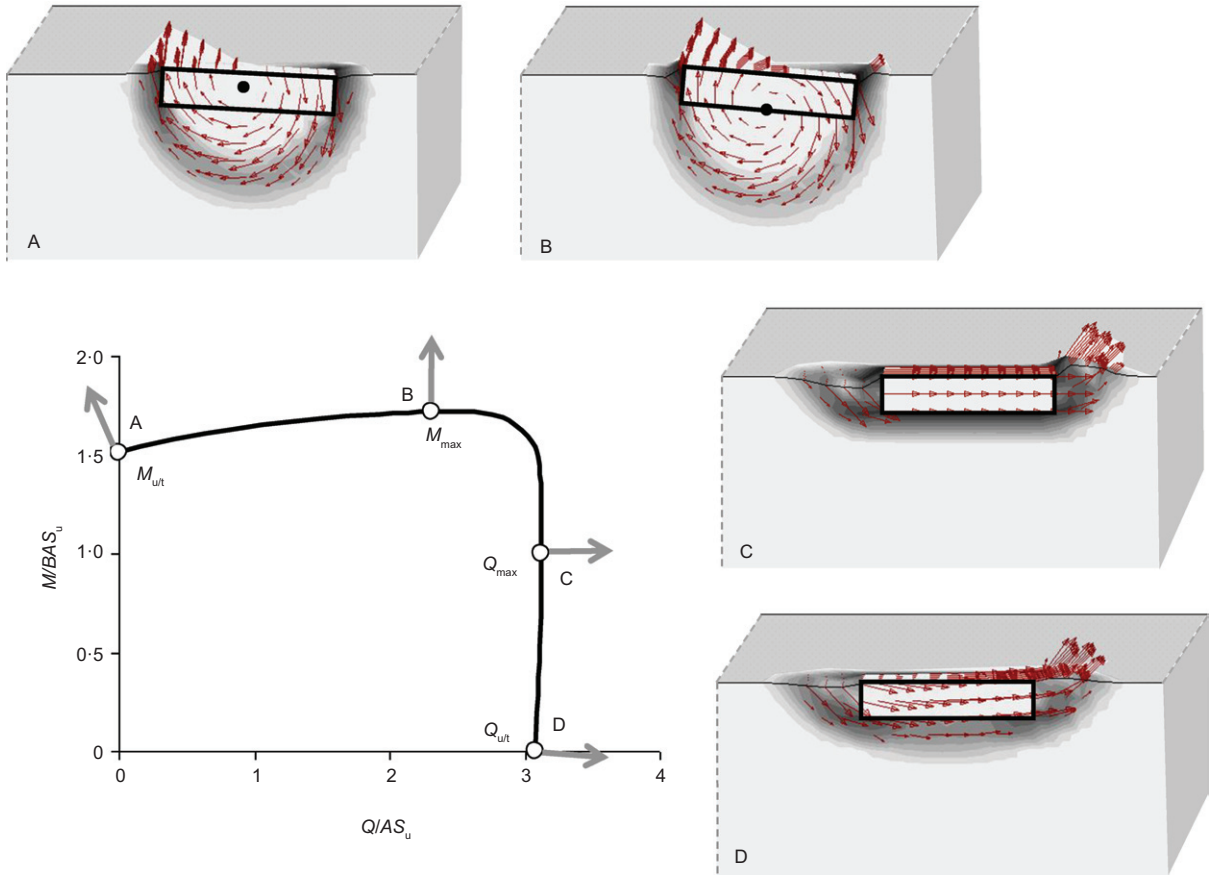

Fig. 10. Graphical representation of MQ interaction envelope with the direction of plastic deformations at four key points. Four offset diagrams show displacement vectors and concentration of shear strains revealing the failure mechanisms at these points. FBC, $D/B=0{\cdot}2$. The solid dots in the pictures represent the instantaneous rotation pole of the foundation. (The pole is at infinity for the horizontal translation case, point C, and 'almost' infinity at point D.)

extent – one-fourth (1/4) to one-eighth (1/8) of the width B (Poulos & Davis, 1974). In contrast, force loading (in shear or normal mode) produces 'stress bulbs' that go much deeper – one to two times the width, respectively. But smaller affected area means smaller total displacements–rotations, and therefore larger stiffnesses. Hence, the sidewalls in rotational modes exhibit much greater stiffness than in translational modes; this explains the trend of Table 1. The difference between the two modes of loading is even larger in the 2D plane-strain problem. The reason: the sidewalls are (infinitely long) strips in this case, possessing negligible stiffness in force loading (theoretically, zero), but offer appreciable stiffness in rocking about the long horizontal axis.

FAILURE ENVELOPES

MQ *interaction (with* N=0*)*

So far, aspects of the maximum horizontal load Q_{max} and of the maximum overturning moment M_{max} have been studied separately. Of course, it was a combination of Q and M that led to these two limit values: a moment was necessary to nullify the rotation as required for Q_{max} and a horizontal force to nullify the horizontal displacement as required for M_{max}. But these were merely two MQ combinations out of infinite possibilities. The full interplay between the limiting values of Q and M, comprising all combinations, is portrayed in Figs 9(a) and 10, in the normalised form: M/BAS_u plotted against Q/AS_u for two values of D/B, 1 and 0·2. The vertical load, N, which also affects the QM interaction, is taken as 0 in both figures. Figure 9(b) is only meant to illustrate the fact that the shape of the failure envelopes depends strongly on the point which M, Q, u and θ refer to. Of course, the information conveyed by each of the three different sets of envelopes (interaction diagrams) for the three reference points (base, middle, top) is exactly the same.

In Figs 9(a) and 10 the location of Q_{max} and M_{max} is shown at the two extremes of the envelope, where the normal lines to the envelope (the 'failure surface') are parallel to the horizontal and vertical axes, respectively. This is a consequence of the associated flow rule adopted in the present soil constitutive model (preservation of normality). Also indicated in the figures are the two limit values of the purely horizontal-force ($M=0$) and purely overturning-moment ($Q=0$) loading, denoted as Q_{ult} and M_{ult}, respectively (adopting the terminology of Gourvenec). The normal vectors to the envelope at these latter locations point to the

negative M and Q axes, respectively – indicative of negative (counter-clockwise) rotation and negative (on the x-axis) displacement, respectively. This behaviour can be visualised in the inserted four snapshots of the vectors of displacement (with the concentration of plastic shear strains superimposed as shadows), for each of the four limit loads discussed here. They correspond to pure horizontal load, pure horizontal translation, pure moment and pure rotation, respectively.

Figures 9(a) and 10 reveal a significant effect of embedment, not only on the values of the various limit loads but also on the shape of the envelope; the latter becomes increasingly skewed with increasing (relative) depth, D/B. As a result, the maximum moment capacity M_{max} (which occurs in the presence of positive horizontal load, applied always at the base) increases disproportionately more than the increase of M_{ult}. Indeed, the ratio M_{max}/M_{ult} attains (approximately) the values of

(*a*) 1·75 for $D/B=1$
(*b*) 1·10 for $D/B=0{\cdot}2$

Similar are the trends of the Q_{max}/Q_{ult} ratio, which is equal to

(*a*) 1·60 for $D/B=1$
(*b*) 1·02 for $D/B=0{\cdot}2$

For the surface foundation, that is, $D/B=0$, both ratios approach 1, as there is negligible coupling of M and Q under fully bonded contact and $N=0$, as considered here.

To further elucidate the role of embedment on the *shape* of the QM failure envelopes, Fig. 11 compares the four envelopes (for $D/B=0$, 0·2, 0·5 and 1) as plotted in the normalised coordinate system: M/M_{ult} plotted against Q/Q_{ult}.

It is also worth observing the failure mechanisms at Q_{ult} and M_{ult} in the inserts in Figs 9 and 10. Under pure moment loading, at M_{ult}, applied at the foundation base level, a scoop mechanism is observed with its rotation pole (indicated with the solid dot in the figure) located approximately $D/2$ above the base, that is, at the foundation centre of gravity. The foundation response is therefore mainly rotational, but it is also accompanied by a negative horizontal translation. The latter, as indirectly evidenced by the oblique intersection of the failure envelope with the moment ordinate axis, is substantial only for the deeper foundation ($D/B=1$); it is of marginal importance for the shallow foundation ($D/B=0{\cdot}2$), and would hardly exist for a surface foundation.

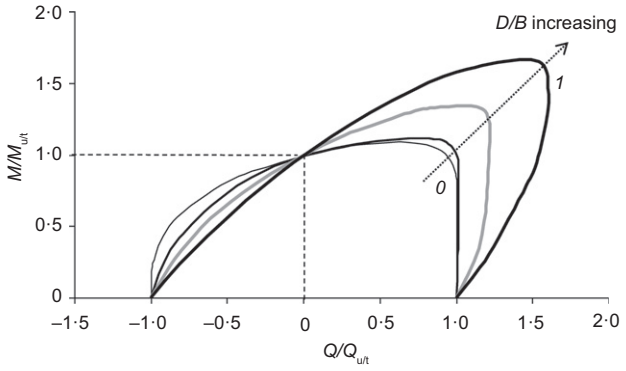

Fig. 11. Normalised MQ interaction envelopes for four embedment ratios $D/B=0$, 0·2, 0·5, 1. FBC, $N=0$

On the contrary, under purely horizontal loading, at Q_{ult}, a reverse scoop mechanism is formed with its centre of rotation moving up near the soil surface – nearly a pendulum. Thus, failure consists of (nearly equally important) horizontal translation and counter-clockwise rotation. In this case, the obliquity of the intersection of the envelope with the Q axis is appreciable even for the shallow foundation ($D/B=0{\cdot}2$).

At the limiting value Q_{max} of exclusively horizontal displacement, the failure mechanism is quite different: sliding of the foundation–soil system develops, with active and passive failure on the front and back side of the foundation, and shear at the base and at the two parallel sidewalls, as already discussed. (Notice in passing the nearly circular (in cross-section) failure mechanisms on both the active and passive sides, justifying the simplified mechanism invoked in the preceding section to obtain equation (9).) At the limit value for pure rotation, M_{max}, the failure mechanism is composite: spheroidal failure surface below the base, active and passive wedges on the upper part of the normal sidewalls, and torsional shear on the parallel sidewalls.

QN *interaction (with* M$=0$*)*

The significance of the vertical load for the ultimate value Q_{ult} of a solely horizontal lateral load ($M=0$) is portrayed in Fig. 12, for four values of D/B: 0, 0·2, 0·5, 1. More specifically: in Fig. 12(a) in the form of Q_{ult}/AS_u plotted against N/AS_u and in Fig. 12(b) in the normalised form $Q_{ult}/Q_{ult,N=0}$ plotted against $N/N_{ult,Q=0}$. Also plotted in Fig. 12(a), for a mere comparison, are the corresponding 2D curves of Gourvenec (2008) for the strip foundation (in which case $A=B$). Observe in Fig. 12(b) that the differences between the normalised curves as functions of D/B are barely if at all distinguishable; also indistinguishable would be the square (3D) and strip (2D) normalised curves (and which are thereby not shown) – proofs of nearly identical shapes of envelopes for both types of foundations (strip and square) and all embedment ratios!

Note in Fig. 12 that for low vertical loads compared to the vertical capacity, $N/N_{ult,Q=0}<0{\cdot}5$, or equivalently for safety factors FS_V against vertical bearing capacity mobilisation exceeding 2 (a most frequent situation in practice), the horizontal capacity remains almost constant, regardless of the axial force magnitude. This is true for all examined embedment ratios. However, an abrupt reduction in load-carrying capacity is noticed at higher vertical loads, with $Q_{ult}/Q_{ult,N=0}$ dropping to about 0·5 for an (admittedly very small) $FS_V=1{\cdot}11$ (i.e. $N/N_{ult,Q=0}=0{\cdot}9$).

MN *interaction (with* Q$=0$*)*

The significance of the vertical load for the ultimate value M_{ult} of a purely moment loading ($Q=0$) is portrayed in Fig. 13, for four values of D/B: 0, 0·2, 0·5, 1. More specifically: in Fig. 13(a) in the form of M_{ult}/ABS_u plotted against N/AS_u and in Fig. 13(b) in the normalised form $M_{ult}/M_{ult,N=0}$ plotted against $N/N_{ult,M=0}$. Also notice in Fig. 13(a), for a mere comparison, the corresponding 2D curves of Gourvenec (2008) for the strip foundation (in which case $A=B$). Again, in Fig. 13(b) the strip (2D) normalised curves would be indistinguishable from the 3D ones if they were shown – proof of nearly identical shapes of the envelopes for both types of foundations and for all studied embedment ratios!

Now the vertical load plays a slightly greater role than for the horizontal capacity. Again, at low values of $N/N_{ult,M=0}$ the effect of N on the M_{ult} is negligible, but the limit now is $N/N_{ult,M=0}<0{\cdot}3$ rather than 0·5. This is true also for all examined embedment ratios. However, an abrupt reduction

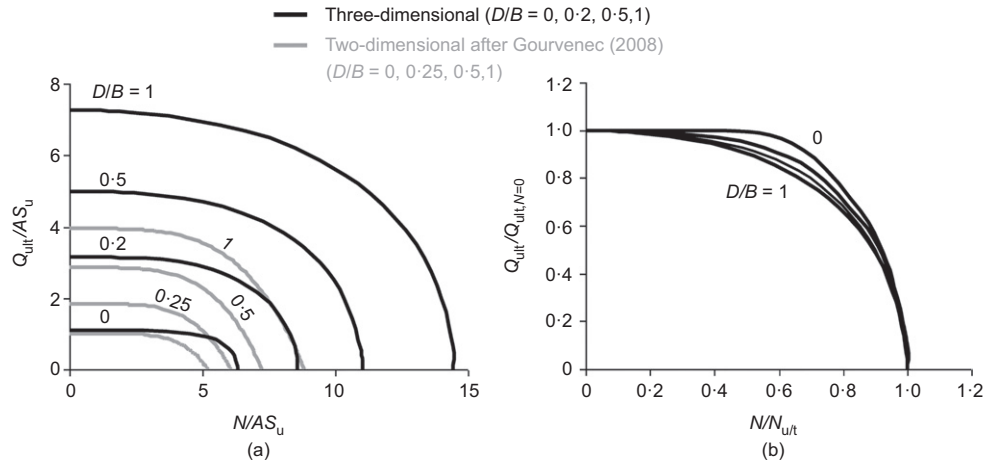

Fig. 12. Three-dimensional embedded-square foundation with FBC compared with Gourvenec's (2008) plane-strain *QN* envelopes normalised: (a) with AS_u and (b) with the ultimate values of *N* and *Q*

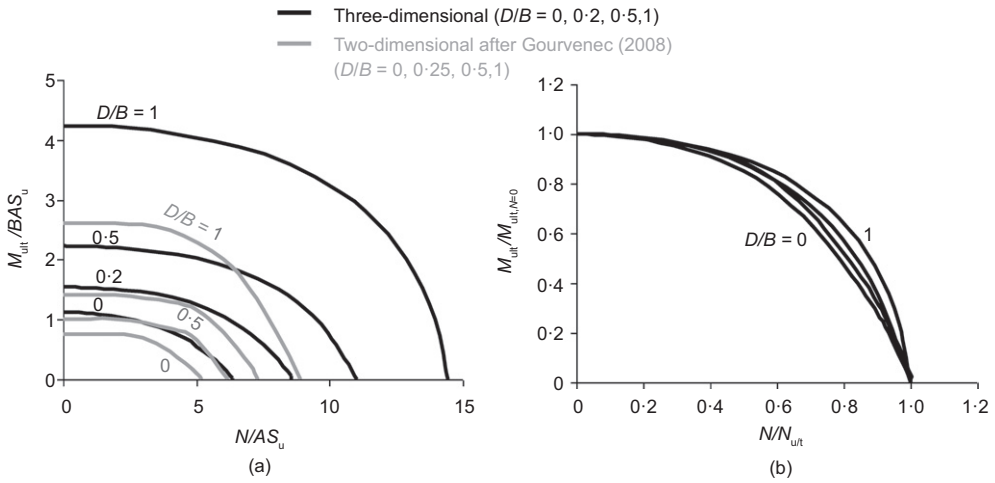

Fig. 13. Three-dimensional embedded-square foundation with FBC compared with Gourvenec's (2008) plane-strain *MN* envelopes normalised: (a) with ABS_u and (b) with the ultimate values of *N* and *M*

in load-carrying capacity is noticed at higher vertical loads, with $M_{ult}/M_{ult,N=0}$ dropping to about 0·5 for the very small $FS_V = 1{\cdot}25$ (i.e. $N/N_{ult,M=0} = 0{\cdot}8$).

TENSIONLESS, POTENTIALLY SLIDING INTERFACE (TSI)

MQ *envelopes with* $N \approx 0$

A very substantial reduction of the effects of embedment ensues when the five interfaces of the foundation with the soil are incapable of transmitting (net) tensional normal stresses and shear stresses that exceed the adhesive stress $f_S = \alpha S_u$. Hence, separation as well as sliding of parts of the walls or the base from the surrounding and underlying soil is a possibility.

Figure 14 shows the *MQ* envelope for the $D/B = 1$ for a foundation with TSI, along with the snapshots of the displacement vectors and the high plastic shear strain 'shadows'. This figure should be compared with Fig. 9 for the same foundation but with FBC, to get an idea of the effects of separation and sliding. Notice the following points. (*a*) For all combinations of *Q* and *M* the limiting values of Fig. 14 decrease due to TSI, and the skewedness of the envelopes seen in Fig. 9 substantially diminishes, being barely distinguishable for the smallest embedment ratios, $D/B = 0{\cdot}2$, examined. (*b*) The failure mechanisms at the four limit points (A–D) seem to consist of only a part of the mechanisms of the FBC analysis of Fig. 9 since, as a consequence of separation, failure is restricted locally in the close vicinity of the particular interface. For instance, at point C of Q_{max} all the back side of the wall loses contact with the soil, and thus no active wedge develops.

At point B of the $D/B = 1$ foundation, corresponding to M_{max}, the TSI mechanism in front and back of the normal-to-loading-direction sidewalls, as well as the one below the base, are almost half (in a qualitative sense) of the FBC mechanisms. The separation of the back wall is due to the combined effects of the clockwise moment $M = M_{max}$ and the positive *Q* required for keeping the base horizontal translation equal to 0.

On the other hand, at the M_{max} point B of the $D/B = 0{\cdot}2$ foundation, the TSI mechanism is altogether different: instead of the scoop mechanism of the FBC foundation of Fig. 9, a Brinch–Hansen-type (1953) wedge is evident.

Figure 15 compares the dimensionless *MQ* envelopes from the FBC and the TSI analyses, for the four D/B ratios (0, 0·2, 0·5, 1). This graph refers to a relatively small but non-zero value of vertical load ($N/N_{ult} = 0{\cdot}25$) to allow comparison with the $D/B = 0$ foundation. In the case of the TSI analysis,

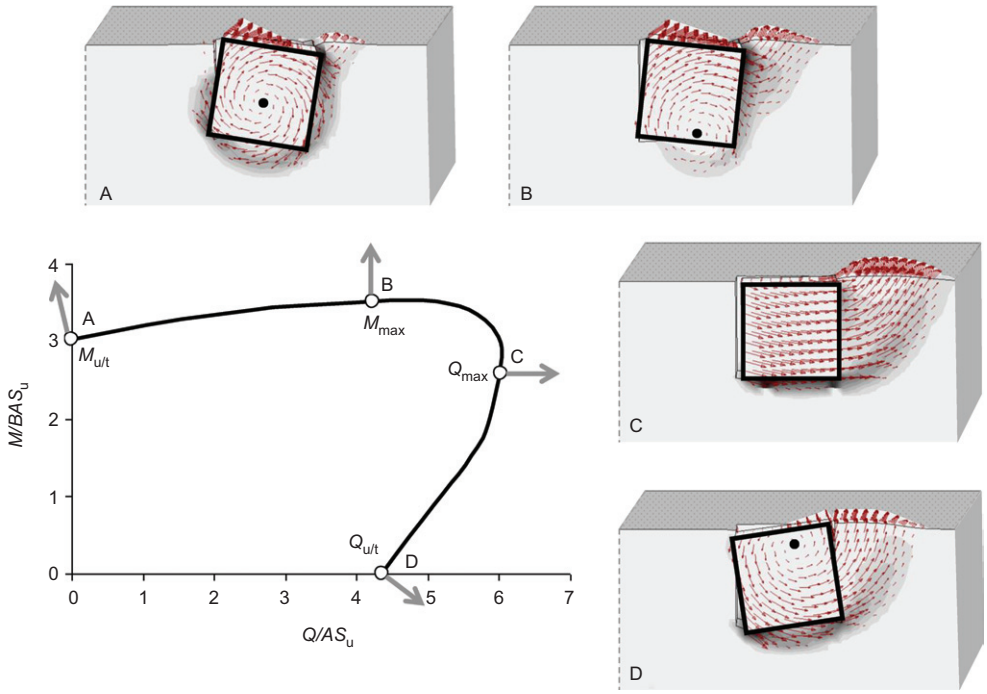

Fig. 14. *MQ* interaction (for $N/N_{ult}=0$): failure mechanisms at key points of the failure envelope of a $D/B=1$ foundation having a tensionless sliding interface (TSI) with the soil. The solid dots represent approximately the instantaneous rotation pole, which for purely horizontal translation (point C) is at infinity

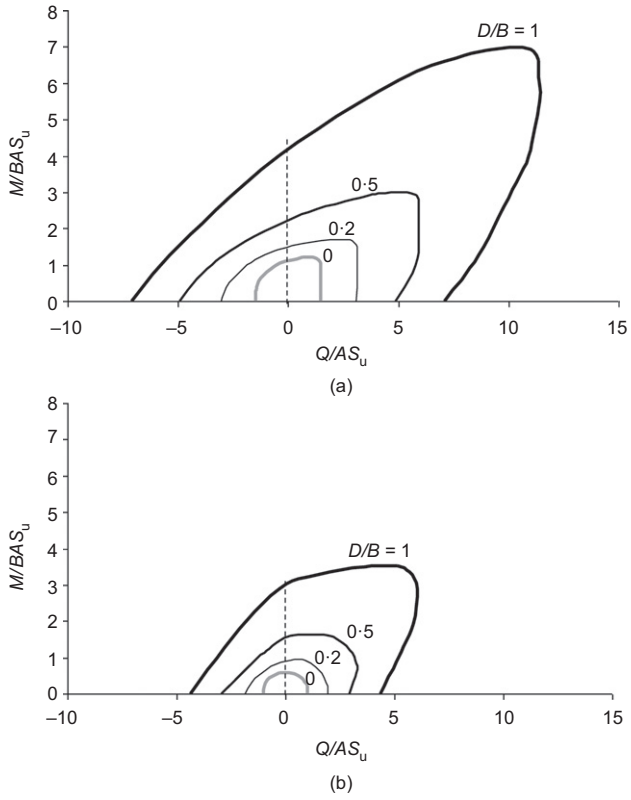

Fig. 15. Effect of interface conditions: failure envelopes in *MQ* load plane for $N/N_{ult}=0{\cdot}25$: (a) FBC, compared to (b) tensionless sliding interface (TSI)

such comparison would not be possible for $N/N_{ult}=0$. This comparison shows that the TSI curves are not only much 'contracted' compared to the FBC curves, but their shapes are also quite different, with the skewness having almost disappeared.

Moment against angle of rotation; soil reactions ($u=0$, $N\neq 0$)

Although the ultimate capacity (moment or horizontal) of an embedded foundation under undrained conditions is only marginally affected by the vertical load, N, as long as the latter does not exceed 1/2 to 1/3 of the vertical bearing capacity, $N_{ult}=N_{ult,M=Q=0}$, it is worth studying the complete moment–rotation curves for a very large factor of safety and for more usual factors of safety: $FS_V=N_{ult,M=Q=0}/N=14$ and 3, representing lightly loaded foundations (or strong soil) and heavily loaded foundations (or weak soil), respectively. The two curves are plotted in Fig. 16. In both cases, the total resisting moment initially increases linearly with rotation angle. The corresponding zero-angle-of-rotation stiffnesses are only very slightly different (difficult to discern in the scale of the figure), because, as was quantitatively shown by Gazetas *et al.* (2013) and Adamidis *et al.* (2014), the heavily loaded (in the vertical direction) foundation induces more plastic deformation in the underlying soil and hence depresses slightly even its lateral effective stiffness. But as soon as initiation of either separation/sliding at the interfaces, or soil yielding, or both, take place, a gradually softening rocking behaviour is observed until the resisting moment reaches its maximum value. Overall, the behaviour of the two foundations is quite similar.

The distribution of soil reactions on the foundation walls is also portrayed in this figure, for four different stages of loading. Only normal stresses are shown on the two vertical walls (front and back) and the base.

At loading points A, compressive and tensile stresses develop along the foundation periphery. Superimposed on the static (gravity-induced) compressive earth pressures they result in an increase of normal stresses in the compression area and a decrease of stresses in the tension area. In the upper half of the back wall, because of the interface's inability to sustain pure tension, separation seems to have already occurred at very small angles of rotation. By the time points B are reached, the above picture has become clearly distinguishable.

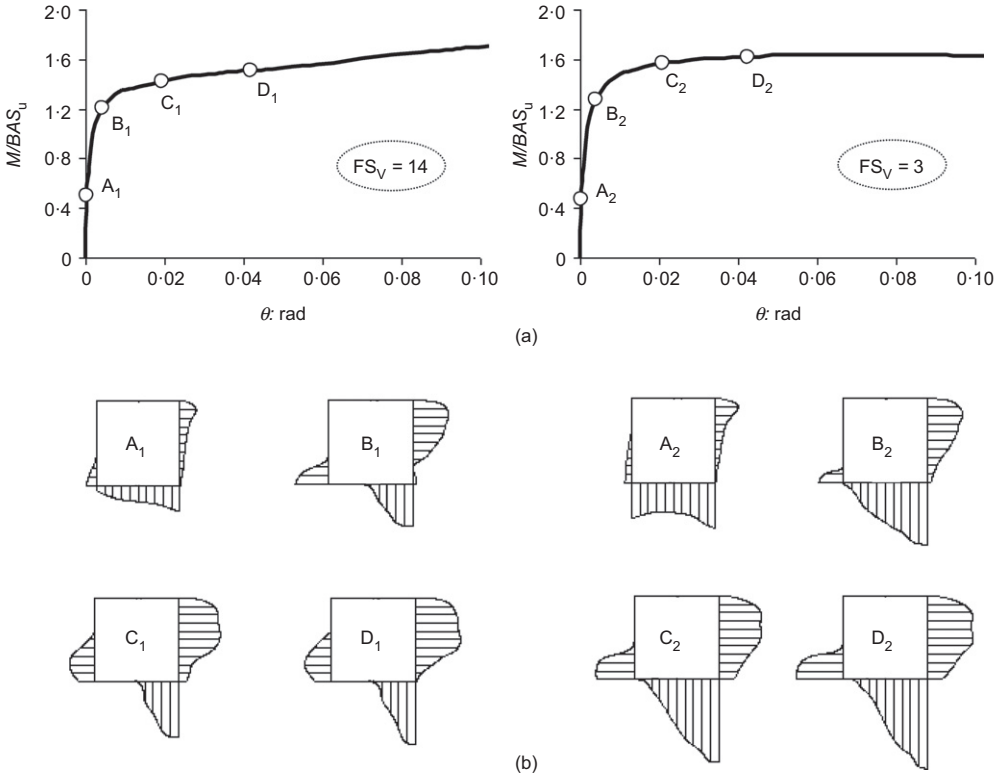

Fig. 16. Illustration of the evolution of stresses at the soil–foundation tensionless sliding interface (TSI) for two different axial loads corresponding to FS_V values of 14 and 3: (a) moment–rotation curves with selected four loading levels; (b) stress distribution at these four levels

As the load increases (points C), ultimate soil reactions seem to have been mobilised near the top of the front sidewall and near the bottom of the back sidewall, similarly on the two foundations. The separation of the back sidewall from the soil has gone deeper in both cases. However, the response at the bases of the heavily and the lightly loaded foundations differ substantially: uplifting of half the base takes place under light (vertical) loading, while compression is still transmitted under the whole heavily loaded base. This is reminiscent of the response of surface foundations that has been amply demonstrated both theoretically and experimentally (Paolucci *et al.*, 2008; Anastasopoulos *et al.*, 2010a, 2012; Deng & Kutter, 2012): uplifting dominates with large FS_V, whereas soil yielding and failure mechanisms dominate with small FS_V.

With further increase in imposed rotation, the contact areas of the sidewalls become somewhat larger (a small reversal of the previous trend) and the soil reactions increase. The base remains almost in full contact (even if barely) under the heavy load. Also unchanged is the area of uplifting of the base under the light load (half of the base remaining in contact). One can appreciate that there is a more-or-less stable distribution of soil stresses beyond point D, in both cases.

CYCLIC LOADING AT LARGE DEFORMATIONS

Rotational response for slender structures: surface foundation

All the results in this section refer only to the non-linear TSI. In general, the response of foundations under strong lateral cyclic loading coming from the superstructure involves rocking, swaying and settlement. Any of these modes can be significant, but for slender structures (say, with $h/B > 1$) rotation dominates over horizontal translation. Thus, to simplify the picture of cyclic response, purely horizontal displacement is not discussed here.

In this section the authors explore the significance of embedment (D/B) on the cyclic rotational ('rocking') behaviour not just of an isolated foundation, but rather of a foundation supporting a simple rigid structure of weight W located at a height h from the foundation top. With tensionless and potentially sliding soil–foundation interfaces (TSI), in addition to the amplitude of loading, the main parameters to investigate are the vertical static factor of safety, FS_V, and the slenderness ratio, h/B; recall Fig. 1(b). A rotation-controlled loading is applied to the structure–foundation system. The loading protocol shown in Fig. 17 comprises six cycles of progressively increasing angle of rotation θ from 0·0025 rad to 0·08 rad (i.e. 2·5 to 80 millirad), covering the range from quasi-linear to highly non-linear response. The rotation is imposed applying a lateral displacement at the mass, as shown in Fig. 1(b). The mass is adjusted appropriately in order to achieve the desired FS_V for each case studied. Constant-amplitude multi-cycle tests have also been performed.

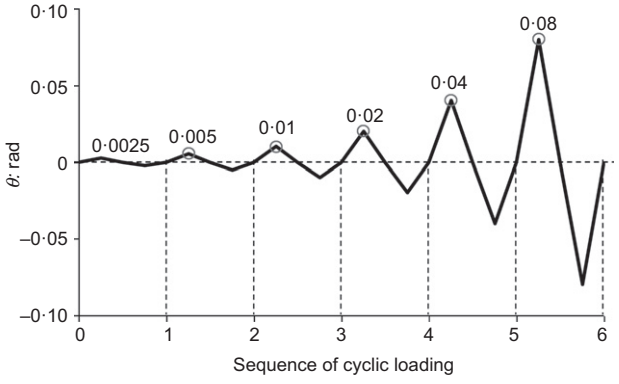

Fig. 17. Cyclic loading protocol (for Figs 18–21)

Developed dimensionless moment–rotation (M/BAS_u plotted against θ) curves now refer to the base of the structure rather than of the foundation, as was the case until now. These curves are presented along with the corresponding dimensionless settlement–rotation (w plotted against θ) curves as follows: in Figs 18 and 19 for surface foundations ($D/B=0$), and in Figs 20 and 21 for embedded foundations with $D/B=0{\cdot}5$ and 1. Two FS_V values are explored: 5 and 2, representing, respectively, lightly loaded structures (or strong soil) and heavily loaded structures (or soft soil). The slenderness ratio, h/B, is varied parametrically ($=1$ and 3) for the surface foundations, but is kept constant ($=1$) for the embedded ones.

For the surface footings, Fig. 18 for the very slender supported structure ($h/B=3$) shows a decline of the monotonic ('backbone') curves after the ultimate moment has been reached, for both FS_V values. This decline is a consequence of the P–Δ effect which stems from the additional moment $\Delta M = W(h \sin\theta)$ generated by the eccentricity of the weight of the structure W as it displaces horizontally by $h \sin\theta \approx h\theta$. ΔM aggravates the consequences of loading, leading to a post-peak decline of the moment capacity. Of course, the phenomenon is conspicuous only at large angles of rotation; it is barely distinguishable at relatively small angles, even after slight exceedance of the maximum moment, as could be seen in this figure (and will be more obvious in the next figures). And as will be shown later, P–Δ is significant mainly for surface (or very shallow) foundations. It is particularly significant for a relatively rigid structure on a rigid base (Makris & Roussos, 2000; Apostolou *et al.*, 2007; Panagiotidou *et al.*, 2012).

A broad similarity is noted in the shape of the two (static) monotonic curves, although the heavily loaded footing ($FS_V=2$) experiences larger moment capacity, as of course was expected even from the Meyerhof bearing capacity solution, but reaches the overturning angle ($\approx$011 rad, where the curve crosses the 0 axis) sooner than that of the lightly loaded $FS_V=5$ foundation ($\approx$019 rad at the projection of the curve).

In both cases the monotonic curves clearly 'envelop' the loops of the (slow) cyclic tests. Hence, the MQN interaction diagrams presented in the paper are also valid for cyclic loading – an important conclusion. Yet, despite their similarities, the two different FS_V foundations behave distinctly differently.

(*a*) An uplifting-dominated behaviour is noted with the lightly loaded foundation ($FS_V=5$), as evidenced indirectly from the roughly-S-shaped M–θ loops (with negligible residual moment each time the imposed rotation returns to 0, implying a 're-centring' capability under cyclic excitation), and directly from the upward displacement of the foundation centre seen in the w–θ curves. Of course, despite such uplifting (or perhaps because of it) there is a progressive recession (permanent loss of contact) between the soil and the foundation under the edges, which leads to the eventual accumulation of a very small (downward) settlement, and to an appreciable degradation of rotational stiffness. (The latter is seen in the decreased slope of the unloading–reloading lines.)

(*b*) A sinking-dominated response is noted with the heavily loaded foundation ($FS_V=2$), as evidenced indirectly from the roughly-O-shaped large inelastic loops in M–θ, and directly from the accumulating downward displacement in the w–θ curves – both phenomena being a consequence of extensive cyclic soil inelastic action.

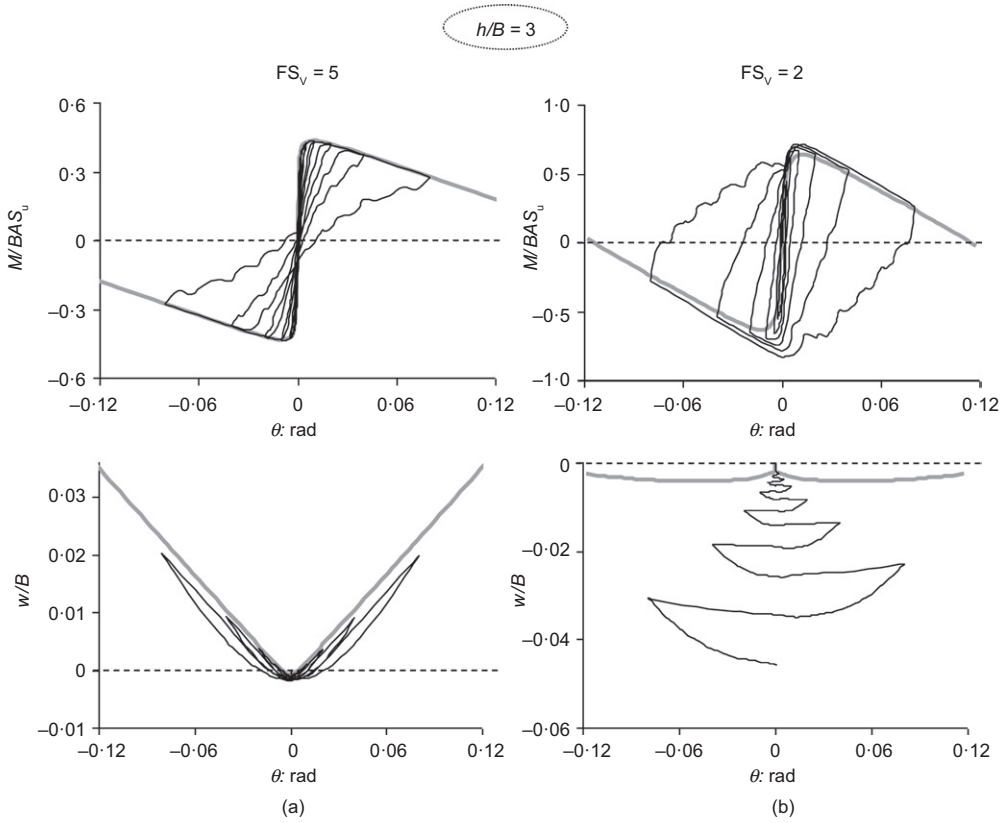

Fig. 18. Dimensionless moment–rotation and settlement–rotation response of a surface TSI foundation subjected to cyclic lateral loading: (a) $FS_V=5$; (b) $FS_V=2$ (grey line corresponds to monotonic backbone curves). $D/B=0$, $h/B=3$

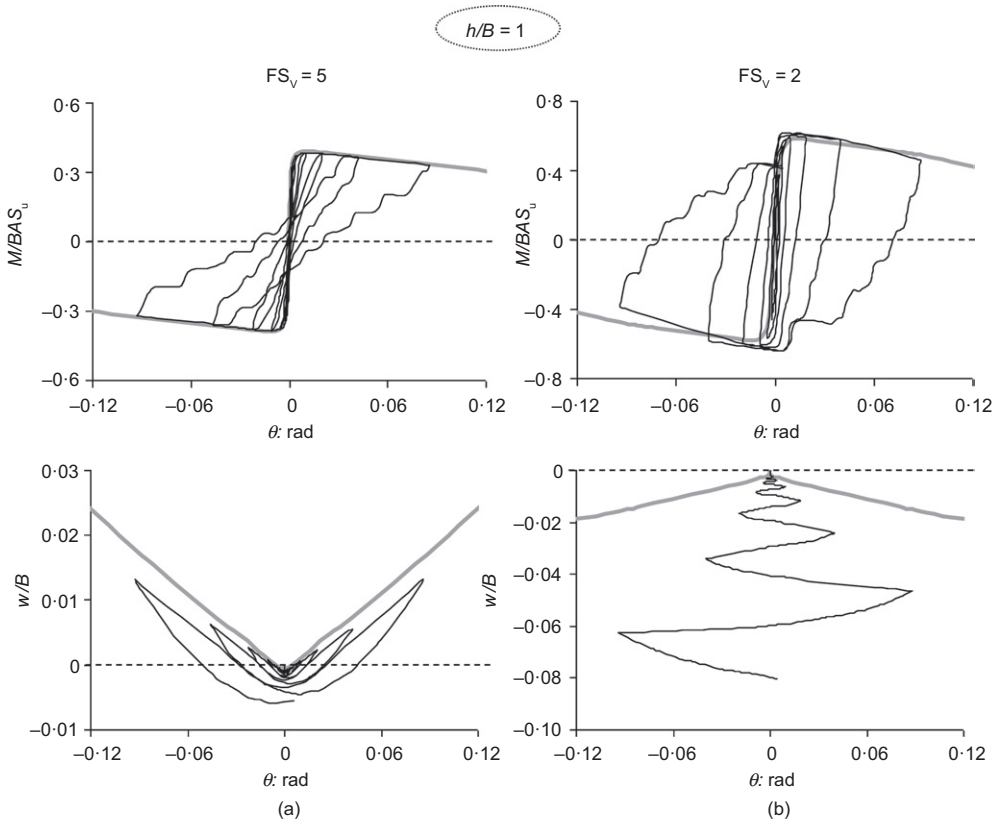

Fig. 19. Dimensionless moment–rotation and settlement–rotation response of a surface TSI foundation subjected to cyclic lateral loading: (a) $FS_V = 5$; (b) $FS_V = 2$ (grey line corresponds to monotonic backbone curves). $D/B = 0$, $h/B = 1$

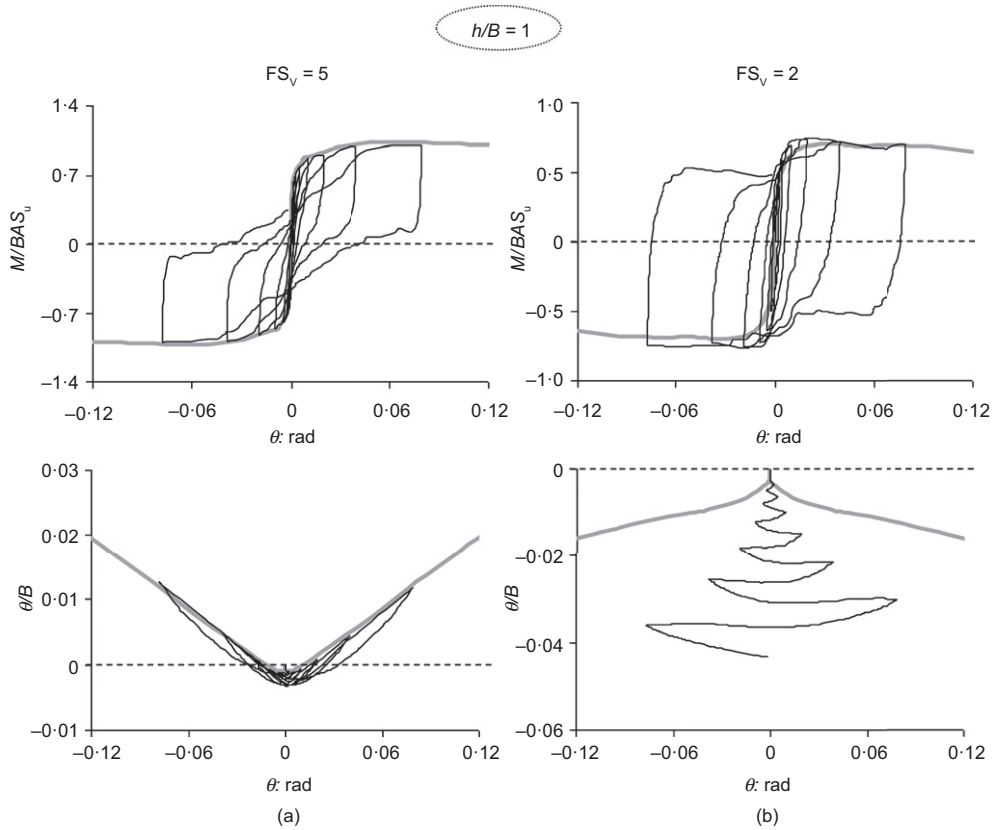

Fig. 20. Dimensionless moment–rotation and settlement–rotation response of a $D/B = 0{\cdot}5$ embedded TSI foundation subjected to cyclic lateral loading: (a) $FS_V = 5$; (b) $FS_V = 2$ (grey line corresponds to monotonic backbone curves). $h/B = 1$

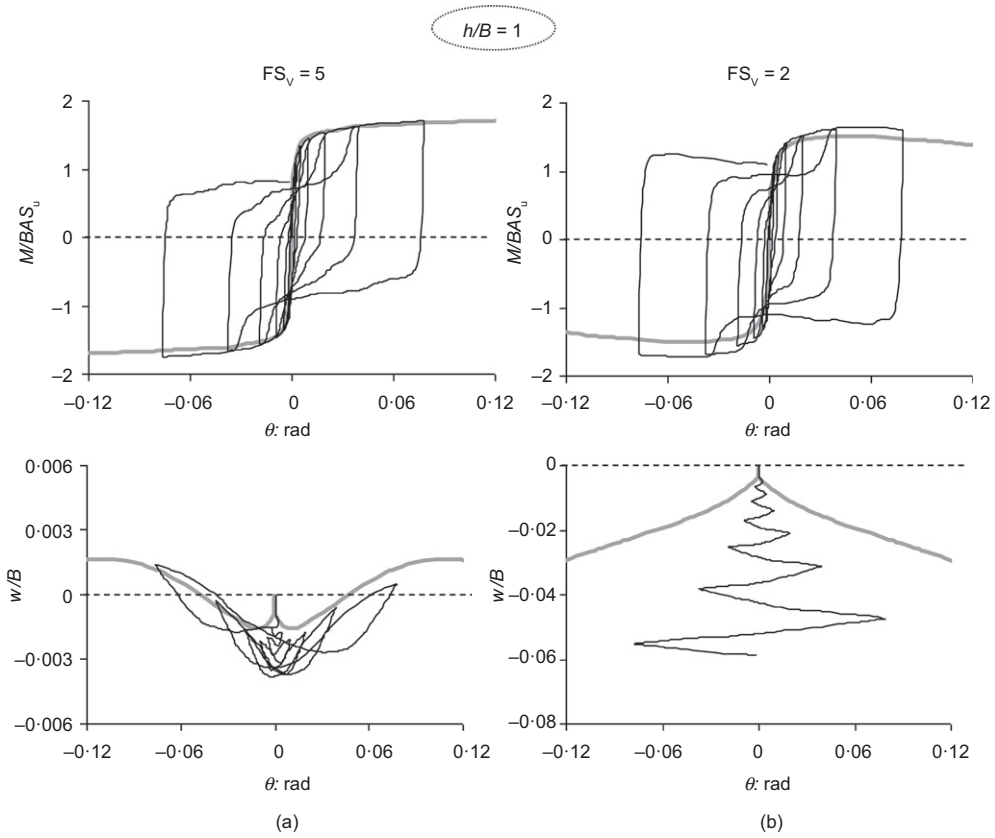

Fig. 21. Dimensionless moment–rotation and settlement–rotation response of a $D/B=1$ embedded TSI foundation subjected to cyclic lateral loading: (a) $FS_V=5$; (b) $FS_V=2$ (grey line corresponds to monotonic backbone curves). $h/B=1$

The less slender system with $h/B=1$ is studied in Fig. 19. In general, the response of the two foundations is similar with that of the corresponding foundations of the very slender system in Fig. 18. The main differences are: the P–Δ effects are in this case (understandably) less prominent, as $W(h\sin\theta)$ is reduced; the S-shape of the M–θ loops for $FS_V=5$ are not as narrow at the centre; and the accumulated settlements are larger for both foundations ($FS_V=2$ and 5). The latter may come as a surprise (less settlement for the taller structure (of the same weight)), but it is a natural consequence of the type of applied loading: for an imposed large angle of rotation, the total moment atop the foundation is about the same in the two cases ($h/B=1$ and 3); however, the contribution to this moment of the (vertical) weight W (P–Δ effect) is 3 times larger for the taller ($h/B=3$) structure, and thereby the corresponding moment due to the horizontal force is 3 times smaller. Therefore, the horizontal shear force $Q=M/h$ developing atop the foundation of the taller system is somewhat smaller than the one coming from the shorter one. Hence in the latter case, the increased Q leads to greater inelastic action in the soil, resulting in greater residual settlement.

The effect of embedment

Figures 20 and 21 show the effect of embedment ($D/B=$ 0·5 and 1) for $h/B=1$ (only), and $FS_V=5$ and 2, as before. The following points may be noticed.

(*a*) The monotonic backbone curves now barely show a sign of P–Δ induced degradation up to an angle of rotation of 0·12 rad; just a 'suspicion' of a decline with the heavier load.

(*b*) The shape of the cyclic moment–rotation loops deviates from that of the surface foundations as embedment increases. Lateral loading of the embedded foundation causes excessive plastic deformation of soil on one side with a gap opening on the opposite side. An abrupt decrease in M upon unloading is attributed to this partial detachment ('gapping effect'), because momentarily both front and back of the sidewalls are not in contact. Upon reversal, contact is re-established and moment resistance slowly increases. Re-centring of the foundation results in a partial loss of contact between the sidewalls and the soil, as the plastically deformed soil is not restored to its original state.

(*c*) With increasing number of loading cycles, the soil–foundation gap, alternately forming on either side of the foundation, progressively widens. This results in a decreased resisting moment during unloading and reloading. Notice that the monotonic curve is reached only when the complete passive earth pressures come into action. Thus, an abrupt increase in M occurs every time the system approaches the angle of rotation corresponding to the amplitude of the previous load cycle.

(*d*) The differences between the lightly and the heavily loaded system in the moment–rotation response become less pronounced as D/B increases. In both cases, the moment–rotation loops reveal a great potential for the soil–foundation system to dissipate a large amount of energy during cyclic loading.

(*e*) Remarkable differences, however, are noticed with respect to the cyclically accumulating settlements as a function of FS_V. The reduced stresses transmitted onto the base soil would be expected to produce less settlement than for surface foundations. In fact, the lightly loaded system ended up with negligible residual settlement for both $D/B=0{\cdot}5$ and $D/B=1$, after the

first few cycles during which the footing alternately uplifted and settled. On the other hand, the heavily loaded system displayed a substantial residual settlement of about $0{\cdot}04B$ for $D/B=0{\cdot}5$ and $0{\cdot}06B$ for $D/B=1$, as its response is characterised by minimal uplifting and excessive soil yielding for the larger angles of rotation.

The effect of loading amplitude on settlement

This is further investigated by imposing five cycles of constant rotation amplitude, $\theta=0{\cdot}0005$, $0{\cdot}0025$, $0{\cdot}02$, $0{\cdot}05$ and $0{\cdot}1$ rad. Four safety factors, $FS_V=14$, 5, 4 and 3, are considered, while $D/B=1$. Thus, a wide range of responses is covered, from nearly elastic to strongly inelastic.

Figure 22 shows the final residual settlement plotted against the imposed rotation amplitude. At relatively small angles of rotation, increasing amplitude implies linearly increasing settlement in all but the very large FS_V case. At larger rotation amplitudes, the rate of settlement increase diminishes, until eventually settlements start levelling off or even decreasing. As a result, at large angles of rotation the lightly loaded systems end up with residual uplift, while the heavily loaded systems end up with reduced settlement. The 'turning point' is a critical angle of rotation, which appears to increase as the factor of safety decreases (for $FS_V=3$ this critical angle has not been reached yet at $0{\cdot}1$ rad.)

SUMMARY AND CONCLUSIONS

The static response of embedded square-in-plan foundations under undrained conditions has been studied with a 3D FE model. Soil (material) inelasticity and soil–foundation interface (geometric and material) non-linearity have been properly taken into account. Emphasis was given to the ultimate capacity under combined lateral (horizontal and moment) loading, but the role of the vertical force was also addressed. Simplified models were developed with the sole purpose of elucidating the phenomena observed numerically. Some attention has been given to the effect of embedment on elastic stiffnesses in pure horizontal translation and pure rotation.

For the (slow) cyclic loading the focus has been on the rotational response of embedded foundations carrying a simple slender structure. Numerical moment–rotation (M–θ) and settlement–rotation (w–θ) loops have been compared with the monotonic curves of the system, with particular emphasis on the importance of the static factor of safety FS_V against vertical ultimate capacity of the foundation. The rotation exceeded substantially the angle of maximum moment capacity of the foundation, and P–Δ effects played their role in function of FS_V and the depth of embedment.

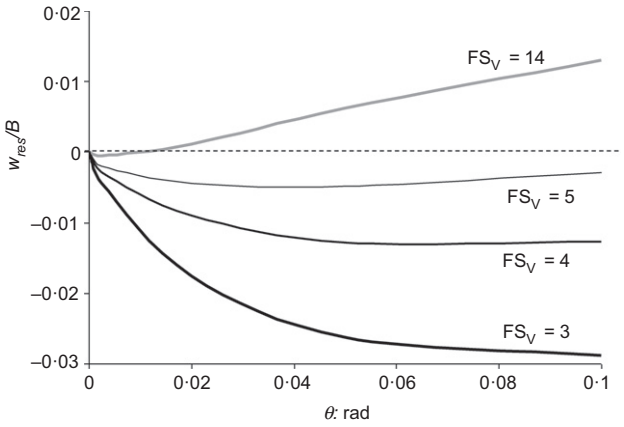

Fig. 22. Dimensionless residual settlement plotted against cyclic rotation amplitude, for a $D/B=1$ embedded TSI foundation (five cycles of constant rotation amplitude θ were imposed)

An interesting finding, which had not been noted explicitly in the literature before, was that the effect of embedment on increasing bearing capacity is much larger than the effect on increasing stiffness: almost four times larger for the horizontal motion and two times larger for rotation. Physical interpretations of these differences have been outlined.

At the soil–foundation interfaces detachment (with subsequent gap formation) and slippage (with shear tractions limited to adhesion) have been shown to exert a rather dramatic effect in reducing the size and even changing the shape of the failure envelops. The relative magnitude of the vertical load affects mainly the uplifting of the base; its effect on the overall ultimate performance is limited.

Along the QM failure envelop of a fully bonded embedded foundation the mechanisms of failure change significantly from point to point. For the four characteristic points, M_{ult}, M_{max}, Q_{max}, Q_{ult}, and an embedment $D/B=1$, the observed mechanisms are, respectively: a clock-wise rotation about a point nearly $2/3$ of D from the top (M_{ult}); a mixed mode consisting of rotation below the base about its centre and of passive- and active-type wedges along the sides normal to the direction of loading (M_{max}); two clear wedges, a passive and an active on each of the two sides, with simple slippage along the base (Q_{max}); and a counter-clock-wise rotation about a point at the top, like a pendulum (Q_{ult}). Of course, the two sidewalls that are parallel to the loading plane experience shear failure in all cases; that may involve mainly torsion, or horizontal and vertical translation, or combinations of these. With the non-linear (tensionless and sliding) interfaces, the mechanisms for the above four loading combinations change mainly due to the detachment that takes place; and the previous symmetry is lost.

The cyclic response of embedded foundations is summarised in the form of foundation moment–rotation (M–θ) and settlement–rotation (w–θ) loops of a rotationally loaded system. The former loops are well enveloped by the corresponding monotonic curves. The latter loops show a small or large accumulation of settlement. The static vertical factor of safety FS_V controls the nature of these loops, perhaps as much as (and in some cases even more than) it affects the value of the ultimate resistance. With high FS_V, interface (geometric) non-linearities prevail, with only minor inelastic (material) action in the soil and hence a small accumulation of settlement with number of cycles. The opposite is true when FS_V is small.

Closed-form expressions for the presented failure envelops (although with the top of the foundation as the reference point) have been given by Ntritsos (2012) and recently by Karapiperis & Gerolymos (2014) and Zafeirakos (2014).

ACKNOWLEDGEMENTS

The financial support for this paper has been provided under the research project 'Dare', which is funded through the European Research Council's (ERC) 'Ideas' Programme, in Support of Frontier Research–Advanced Grant, under contract/number ERC-2-9-AdG228254–DARE. The authors are grateful for the invaluable help of Dr Evangelia Garini in preparing the figures.

NOTATION

$A_{sidewall}$ area of foundation sidewall ($=DB$)
B width of footing
C initial kinematic hardening modulus
c_a cohesion at soil–foundation interface ($=\alpha S_u$)

D embedment depth (=0, 0·2, 0·5, 1 m)
E Young's modulus
E_s undrained Young's modulus of soil ($=1800S_u$)
$F_{sidesoil}$ soil reaction force on vertical sidewalls
FS_V factor of safety against exceeding the purely vertical bearing capacity
f_S limiting shear resistance
G shear modulus
G_o small-strain shear modulus
h height of structural mass from foundation top (= 1 m, 3 m)
K_H elastic horizontal stiffness of an embedded square-in-plan foundation
K_{HO} elastic horizontal stiffness of a surface square-in-plan foundation
K_R elastic rotational stiffness of an embedded square-in-plan foundation
K_{RO} elastic rotational stiffness of a surface square-in-plan foundation
$^{2d}K_H$ elastic horizontal stiffness of an embedded strip foundation
$^{2d}K_{HO}$ elastic horizontal stiffness of a surface strip foundation
$^{2d}K_R$ elastic rotational stiffness of an embedded strip foundation
$^{2d}K_{RO}$ elastic rotational stiffness of a surface strip foundation
M overturning moment
M_{max} maximum moment capacity of an embedded square-in-plan foundation
$M_{T,sidewall}$ torsional moment of the soil reactions on sidewalls
M_{ult} purely moment capacity
M_{uo} maximum moment capacity of a surface square-in-plan foundation
$^{2d}M_{max}$ maximum moment capacity of an embedded strip foundation
$^{2d}M_{uo}$ maximum moment capacity of a surface strip foundation
m mass of superstructure
N vertical force
N_u ultimate vertical load of embedded square-in-plan foundation
N_{ult} purely vertical capacity
N_{uo} ultimate vertical load of a surface square-in-plan foundation
$^{2d}N_{uo}$ ultimate vertical load of surface strip foundation
P_{active} limiting active force
$P_{passive}$ limiting passive force
Q horizontal force
Q_{max} maximum horizontal load of an embedded square-in-plan foundation
Q_{ult} purely horizontal capacity
Q_{uo} maximum horizontal load of a surface square-in-plan foundation
$^{2d}Q_{max}$ maximum horizontal load of an embedded strip foundation
$^{2d}Q_{uo}$ maximum horizontal load of a surface strip foundation
S_u undrained shear strength
T_{base} resultant shear force on the base
$T_{sidewall}$ resultant shear force on the vertical sidewalls
u horizontal translation
W weight of superstructure
w vertical translation (settlement)
α adhesion coefficient
β 'back-stress' parameter
γ parameter determining rate of decrease of kinematic hardening with increasing plastic deformation
δ sidewall displacement
ε_y yield normal strain
θ rotation
λ fraction of yield stress
ν Poisson's ratio
σ_u ultimate strength
σ_y yield stress defined in equation (3)
σ_0 stress defined in equation (5)

REFERENCES

Abaqus (2008). *Theory and analysis user's manual*, *version 6.8-3*. Providence, RI, USA: Dassault Systèmes Simulia Corp.

Adamidis, O., Gazetas, G., Anastasopoulos, I. & Argyrou, C. (2014). Equivalent–linear stiffness and damping in rocking of circular and strip foundations. *Bull. Earthquake Engng* **12**, No. 3, 1177–1200.

Allotey, N. & Naggar, M. H. E. (2003). Analytical moment–rotation curves for rigid foundations based on a Winkler Model. *Soil Dynam. Earthquake Engng* **23**, No. 5, 367–381.

Anastasopoulos, I., Gazetas, G., Loli, M., Apostolou, M. & Gerolymos, N. (2010a). Soil failure can be used for seismic protection of structures. *Bull. Earthquake Engng* **8**, No. 2, 309–325.

Anastasopoulos, I., Georgarakos, T., Georgiannou, V., Drosos, V. & Kourkoulis, R. (2010b). Seismic performance of bar-mat reinforced-soil retaining wall: shaking table testing versus numerical analysis with modified kinematic hardening constitutive model. *Soil Dynam. Earthquake Engng* **30**, No. 10, 1089–1105.

Anastasopoulos, I., Gelagoti, F., Kourkoulis, R. & Gazetas, G. (2011). Simplified constitutive model for simulation of cyclic response of shallow foundations: validation against laboratory tests. *J. Geotech. Geoenviron. Engng, ASCE* **137**, No. 12, 1154–1168.

Anastasopoulos, I., Loli, M., Gelagoti, F., Kourkoulis, R. & Gazetas, G. (2012). Nonlinear soil–foundation interaction: numerical analysis. *Proceedings of the 2nd international conference on performance-based design in earthquake geotechnical engineering*, Taormina, Italy.

Apostolou, M., Gazetas, G. & Garini, E. (2007). Seismic response of slender rigid structures with foundation uplifting. *Soil Dynam. Earthquake Engng* **27**, No. 7, 642–654.

Bilotta, E., Lanzano, G., Madabhushi, S. P. G. & Silvestri, F. (2014). A numerical round robin on tunnels under seismic actions. *Acta Geotechnica* **9**, No. 4, 563–579.

Bransby, M. F. & Randolph, M. F. (1999). The effect of embedment depth on the undrained response of skirted foundations to combined loading. *Soils Found.* **39**, No. 4, 19–33.

Brinch Hansen, J. (1970). *A revised and extended formula for bearing capacity*, Bulletin No. 28, pp 5–11. Copenhagen, Denmark: Danish Geotechnical Institute.

Butterfield, R. & Gottardi, G. (1994). A complete three-dimensional failure envelope for shallow footings on sand. *Géotechnique* **44**, No. 1, 181–184, http://dx.doi.org/10.1680/geot.1994.44.1.181.

Butterfield, R. & Ticoff, J. (1979). Design parameters for granular soils. *Proceedings of the 7th European conference on soil mechanics and foundation engineering*, Brighton, UK, vol. 4, pp. 259–261.

Chatzigogos, C. T., Pecker, A. & Salencon, J. (2009). Macroelement modelling of shallow foundations. *Soil Dynam. Earthquake Engng* **29**, No. 5, 765–781.

Deng, L. & Kutter, B. L. (2012). Characterization of rocking shallow foundations using centrifuge model tests. *Earthquake Engng Structl Dynam.* **41**, No. 5, 1043–1060.

Dobry, R. (2014). Simplified methods in soil dynamics. *Soil Dynam. Earthquake Engng* **61–62**, 246–268. (Also found as: Nabor Carrillo Lecture, Sociedad Mexicana de Ingenieria Geotecnica, 2012.)

Dobry, R. & Gazetas, G. (1986). Dynamic response of arbitrarily-shaped foundations. *J. Geotech. Engng, ASCE*, **113**, No. 2, 109–135.

Faccioli, E., Paolucci, R. & Vivero, G. (2001). Investigation of seismic soil–footing interaction by large scale cyclic tests and analytical models. *Proceedings of the 4th international conference on recent advances in geotechnical earthquake engineering and soil dynamics*, San Diego (ed. S. Prakash), paper no. SPL-5 (CD-ROM).

Gajan, S. & Kutter, B. L. (2008). Capacity, settlement, and energy dissipation of shallow footings subjected to rocking. *J. Geotech. Geoenviron. Engng, ASCE* **134**, No. 8, 1129–1141.

Gazetas, G. (1983). Analysis of machine foundation vibrations: state of the art. *Soil Dynam. Earthquake Engng* **2**, No. 1, 2–43.

Gazetas, G. (1991). Formulas and charts for impedances of surface and embedded foundations. *J. Geotech. Engng*, *ASCE* **117**, No. 9, 1363–1381.

Gazetas, G. (2015). 4th Ishihara Lecture: Soil–foundation–structure systems beyond conventional seismic failure thresholds. *Soil Dynam. Earthquake Engng* **68**, 23–39.

Gazetas, G., Adamidis, O., Anastasopoulos, I. & Kontoroupi, T. (2013). Nonlinear rocking stiffness of foundations. *Soil Dynam. Earthquake Engng* **47**, 83–91.

Georgiadis, M. & Butterfield, R. (1988). Displacements of footing on sands under eccentric and inclined loading. *Can. Geotech. J.* **25**, No. 2, 199–212.

Gerolymos, N. & Gazetas, G. (2006a). Winkler model for lateral response of rigid caisson foundations in linear soil. *Soil Dynam. Earthquake Engng* **26**, No. 5, 347–361.

Gerolymos, N. & Gazetas, G. (2006b). Development of Winkler model for static and dynamic response of caisson foundations with soil and interface nonlinearities. *Soil Dynam. Earthquake Engng* **26**, No. 5, 363–376.

Gerolymos, N. & Gazetas, G. (2006c). Static and dynamic response of massive caisson foundations with soil and interface nonlinearities – validation and results. *Soil Dynam. Earthquake Engng*, **26**, No. 5, 377–394.

Giannakos, S., Gerolymos, N. & Gazetas, G. (2012). Cyclic lateral response of piles in dry sand: Finite element modeling and validation. *Comput. Geotech.* **44**, 116–131.

Gottardi, G., Houlsby, G. T. & Butterfield, R. (1999). The plastic response of circular footings under general planar loading. *Géotechnique* **49**, No. 4, 453–470, http://dx.doi.org/10.1680/geot.1999.49.4.453.

Gourvenec, S. (2007). Shape effects on the capacity of rectangular footings under general loading. *Géotechnique* **57**, No. 8, 637–646, http://dx.doi.org/10.1680/geot.2007.57.8.637.

Gourvenec, S. (2008). Effect of embedment on the undrained capacity of shallow foundations under general loading. *Géotechnique*, **58**, No. 3, 177–185, http://dx.doi.org/10.1680/geot.2008.58.3.177.

Houlsby, G. T. (2003). Modelling of shallow foundations for offshore structures. In *BGA international conference on foundations – innovations, observations, design and practice* (ed. T. A. Newson), pp 11–26. London, UK: Thomas Telford.

Houlsby, G. T. & Puzrin, A. M. (1999). The bearing capacity of strip footings on clay under combined loading. *Proc. R. Soc. A: Math. Phys. Enging Sci.* **455**, No. 1983, 893–916.

Kausel, E. (2010). Early history of soil–structure interaction. *Soil Dynam. Earthquake Engng* **30**, No. 9, 822–832.

Kausel, E. & Roesset, J. M. (1975). Dynamic stiffness of circular foundations. *J. Engng Mech. Div., ASCE* **101**, No. 6, 771–785.

Karapiperis, K. & Gerolymos, N. (2014). Combined loading of caisson foundation in cohesive soil: finite element versus Winkler modeling. *Comput. Geotech.* **56**, 100–120.

Lanzano, G., Bilotta, E., Russo, G., Silvestri, F. & Madabhushi, S. P. G. (2012). Centrifuge modeling of seismic loading on tunnels in sand. *Geotech. Testing J.* **35**, No. 6, 854–869.

Lekkakis, P. (2012). *Analysis of skirted foundations for offshore wind turbines.* Diploma thesis, Laboratory of Soil Mechanics, National Technical University of Athens, Athens, Greece.

Makris, N. & Roussos, Y. (2000). Rocking response of rigid blocks under near source ground motions. *Géotechnique* **50**, No. 3, 243–262, http://dx.doi.org/10.1680/geot.2000.50.3.243.

Martin, C. M. (1994). *Physical and numerical modelling of offshore foundations under combined loads.* DPhil thesis, University of Oxford, Oxford, UK.

Martin, G. R. & Lam, P. (2000). Earthquake resistant design of foundations: retrofit of existing foundations. *Proceedings of the geo-engineering 2000 conference*, Melbourne, Australia.

Meyerhof, G. G. (1953). The bearing capacity of foundations under eccentric and inclined loads. *Proceedings of the 3rd international conference on soil mechanics foundation engineering*, Zurich, Switzerland, vol. 1, pp. 440–445.

Nova, R. & Montrassio, L. (1991). Settlements of shallow foundations on sand. *Géotechnique* **41**, No. 2, 243–256, http://dx.doi.org/10.1680/geot.1991.41.2.243.

Ntritsos, N. (2012). *Inelastic response of embedded foundations.* Diploma thesis, Laboratory of Soil Mechanics, National Technical University of Athens, Athens, Greece.

Pais, A. & Kausel, E. (1988). Approximate formulas for dynamic stiffnesses of rigid foundations. *Soil Dynam. Earthquake Engng* **7**, No. 4, 213–227.

Panagiotidou, A. I., Gazetas, G. & Gerolymos, N. (2012). Pushover and seismic response of foundations on stiff clay: analysis with P–Δ effects. *Earthquake Spectra* **28**, No. 4, 1589–1618.

Paolucci, R., Shirato, M. & Yilmaz, M. T. (2008). Seismic behaviour of shallow foundations: Shaking table experiments vs numerical modeling. *Earthquake Engng Structl Dynam.* **37**, No. 4, 577–595.

Pecker, A. (1998). Capacity design principles for shallow foundations in seismic areas. *Proceedings of the 11th European conference on earthquake engineering*, Paris, France, Invited Lectures volume, pp. 303–316.

Poulos, H. G. & Davis, E. H. (1974). *Elastic solutions for soil and rock mechanics.* New York, NY, USA: John Wiley & Sons.

Poulos, H. G., Carter, J. P. & Small, J. C. (2001). Foundations and retaining structures – research and practice. *Proceedings of the 15th international conference on soil mechanics and geotechnical engineering*, Istanbul, Turkey, vol. 4, pp. 2527–2607.

Randolph, M. & Gourvenec, S. (2011). *Offshore geotechnical engineering*. Abingdon, Oxford, UK: Spon Press.

Randolph, M. & Puzrin, A. M. (2003). Upper bound limit analysis of circular foundations on clay under general loading. *Géotechnique* **53**, No. 9, 785–796, http://dx.doi.org/10.1680/geot.2003.53.9.785.

Roesset, J. M. (1980). Stiffness and damping coefficients of foundations. In *Dynamic response of foundations: analytical aspects* (eds M.W. O'Neil and R. Dobry), pp. 1–30. New York, NY, USA: American Society of Civil Engineers.

Salencon, J. & Pecker, A. (1995). Ultimate bearing capacity of shallow foundations under inclined and eccentric loads. Part II: Purely cohesive soil without tensile strength. *Eur. J. Mech. A – Solids* **14**, No. 3, 377–96.

Tassoulas, J. L. & Kausel, E. (1983). On the effect of the rigid sidewall on the dynamic stiffness of embedded circular footings. *Earthquake Engng Structl Dynam.* **11**, No. 3, 403–14.

Taiebat, H. A. & Carter, J. P. (2000). Numerical studies of the bearing capacity of shallow foundations on cohesive soil subjected to combined loading. *Géotechnique* **50**, No. 4, 409–418, http://dx.doi.org/10.1680/geot.2000.50.4.409.

Terzaghi, K. (1943). *Theoretical soil mechanics.* New York, NY, USA: John Wiley.

Tsinidis, G., Pitilakis, K. & Trikalioti, A. D. (2014). Numerical simulation of round robin numerical test on tunnels using a simplified kinematic hardening model. *Acta Geotechnica* **9**, No. 4, 641–659.

Vucetic, M. & Dobry, R. (1991). Effect of soil plasticity on cyclic response. *J. Geotech. Engng, ASCE* **117**, No. 1, 89–107.

Vulpe, C., Gourvenec, S. & Power, M. (2014). A generalised failure envelope for undrained capacity of circular shallow foundations under general loading. *Géotechnique Lett.* **4**, No. 3, 187–196.

Wolf, J. P. (1985). *Dynamic soil–structure interaction*. Englewood Cliffs, NJ, USA: Prentice-Hall.

Wolf, J. P. (1988). *Soil–structure interaction analysis in time-domain*. Englewood Cliffs, NJ, USA: Prentice-Hall.

Yun, G. & Bransby, M. F. (2007). The horizontal-moment capacity of embedded foundations in undrained soil. *Can. Geotech. J.* **44**, No. 4, 409–424.

Zafeirakos, A. (2014). *Static and seismic inelastic response of deeply embedded foundations.* PhD thesis, Laboratory of Soil Mechanics, National Technical University of Athens, Athens, Greece.